DOE/ET-53088-262 IFSR #262

Sideband Instabilities in Free Electron Lasers

Marshall N. Rosenbluth, H. Vernon Wong
Institute for Fusion Studies
The University of Texas at Austin
Austin, Texas 78712

and

B. N. Moore
Fusion Research Center
The University of Texas at Austin
Austin, Texas 78712

March 1990

Sideband Instabilities in Free Electron Lasers

MARSHALL N. ROSENBLUTH,[a] H. VERNON WONG,
Institute for Fusion Studies
The University of Texas at Austin
Austin, Texas 78712
and
B. N. MOORE
Fusion Research Center
The University of Texas at Austin
Austin, Texas 78712

Abstract

The linear stability of sideband modes for a one-dimensional free electron laser is investigated in detail. The dependence on wiggler taper, slippage between optical pulse and electrons, and trapped electron distribution functions is included in the analysis. Nyquist plots are used to delineate the parameter space in which sideband instabilities occur, and approximate analytic expressions for the linear growth rate derived. In special cases a complete analytic solution is given. Essentially all equilibria are unstable to sideband growth. The linear growth rates agree well with numerical simulations.

[a]Present address: Univ. of California at San Diego, Department of Physics, La Jolla, California 92093

I. Introduction

Electrons trapped in the ponderomotive well of a free electron laser may be subject to a "sideband" instability[1] in which the optical pulse (signal) decays into sideband signals with frequencies displaced from the main signal frequency by the Doppler shifted oscillation ("synchrotron") frequency of the electrons in the ponderomotive well. Generally growth rates are of the order of the synchrotron frequency.

The sideband instability, when it grows to a large amplitude, can lead to detrapping of electrons and reduction of signal gain. This has been observed in simulations[2–11] and also seen experimentally.[12,13] There are some indications that the output of oscillators with untapered wigglers may be slightly enhanced by the presence of sidebands.[4,12] For tapered wigglers which rely on trapping and deceleration to increase efficiency, it may be necessary to provide a narrow band pass optical filter to suppress sideband growth and prevent detrapping or otherwise constrain designs in order to produce a good signal.

The first predictions of this instability[1] were made by looking at the energetics of the interaction without properly taking into account the phase changes in the optical signals which result from the presence of the bunched electrons. In this paper we correct that error (first discussed in 1983 in Ref. 14), which does not in fact turn out to greatly influence the results, and present a general one-dimensional theory[14] for the linear growth rate of sidebands for a steady state equilibrium comprising a monochromatic signal with an arbitrary distribution of trapped electrons for tapered and untapered wigglers. The limit of untapered wigglers has also been analyzed by other authors[15–18] but in less generality. The case of an untapered wiggler with all electrons trapped at the bottom of the well is particularly simple, and for completeness, we include this case in our discussion, and at the same time extend it to tapered wigglers.

We further examine quantitatively a suggestion made by Fawley et al.[19,20] who point out that the simple picture of the sideband instability depends on slippage between optical pulse

and electrons. Hence, if the group velocity of the electromagnetic wave can be reduced (by use of a wave guide for example) to equal the electron longitudinal velocity, the sideband should be suppressed. We will determine that this in fact depends on the trapped particle distribution function and that growth is indeed greatly reduced in many cases, but difficult to completely stabilize. On the other hand, the usual case where slippage occurs is shown to be nearly always strongly unstable in the sense that sideband growth exceeds signal growth.

While the basic Raman physical mechanism is easy to understand, and has been discussed in various references,[2,21] the detailed dependence of the instability linear behavior on the trapped particle distribution function, on the acceleration (deceleration) of the electrons in a tapered wiggler, and on the slippage between electron velocity and e.m. wave group velocity is sufficiently complex as to make physical interpretation difficult. Rather it is the purpose of this paper to present a general mathematical framework for discussion of the problem and to present fairly detailed results on linear sideband instability behavior for a wide range of situations. For simplicity we will study the case of a helical wiggler and a circularly polarized wave. For a plane polarized wiggler, the equations are more complicated since coupling obtains to sideband modes with wavenumber k_z as well as $k_z + 2lk_w$, where l is an integer. We will not consider this case further here, but note that if we make the usual approximation $\Omega/k_w \ll 1$ with Ω the synchrotron oscillation wavenumber and k_w the wiggler wavenumber, then the equations for the plane wiggler become identical to those for the helical wiggler if the electron current is renormalized by a factor

$$\left[J_0\left(\frac{a_w^2/4}{1+a_w^2/2}\right) - J_1\left(\frac{a_w^2/4}{1+a_w^2/2}\right)\right]^2 .$$

We have not investigated more precisely how small Ω/k_w must be in order to validate our approximations for the plane case.

In Sec. II, we derive the linear dispersion relation for sideband instabilities in free electron lasers. This dispersion relation simplifies considerably in the limit of all electrons trapped at the bottom of the pondromotive well, and in Sec. III we analyze this limit in detail. We obtain

sufficient conditions for the stability of sideband modes, and we estimate the magnitude of unstable sideband growth rates. This analysis is repeated for the more realistic case of a distribution of trapped electrons in the ponderomotive well, and it is discussed in Sec. IV for untapered and tapered wigglers. In Sec. V, we describe numerical simulation of unstable sideband modes, and we compare the observed growth rates with the growth rates calculated in the previous sections. Finally, we present a summary of our results in Sec. VI. A Glossary of symbols is given after Sec. VI.

II. Linear Dispersion Relation

A. Electron dynamics

We start from the Hamiltonian for a highly relativistic $\gamma \gg 1$ electron beam. The longitudinal component of electron momentum serves as the Hamiltonian when z is used as the independent variable. In units of mc we have for an electron beam of low emittance (canonical $p_\perp = 0$)

$$P_z \equiv H(t,\gamma,z) = \gamma - \frac{1 + a_w^2 + a_s^2 + 2a_w a_s \cos\left(\omega t - (k_w + k_s)\, z - \xi\right)}{2\gamma}. \tag{1}$$

Here $\mathbf{a}_w = a_w\left[\hat{x}\cos k_w z + \hat{y}\sin k_w z\right]$ and $\mathbf{a}_s = a_s[\hat{x}\cos\left(\omega t - k_s z - \xi\right) + \hat{y}\sin\left(\omega t - k_s z - \xi\right)]$ are the dimensionless $a = \frac{e}{mc^2}A$ vector potentials for the wiggler and radiation fields. We will assume a_s and the wave phase ξ to be slowly varying in space and time. We neglect a_s^2 as being typically very small. The particle equations of motion in terms of the canonical phase space variables t, γ are now easily found from

$$\frac{dt}{dz} = \frac{\partial H}{\partial \gamma} \qquad \text{and} \qquad \frac{d\gamma}{dz} = -\frac{\partial H}{\partial t}. \tag{2}$$

We find (in units $c = 1$)

$$\frac{dt}{dz} = 1 + \frac{1 + a_w^2}{2\gamma^2} + \cdots \tag{3}$$

$$\frac{d\gamma}{dz} = -\frac{a_w a_s \omega}{\gamma}\sin\left(\omega t - (k_w + k_s)\, z - \xi\right). \tag{4}$$

If we define the optical phase $\psi \equiv (k_w + k_s)\, z - \omega t + \pi$, and $\gamma = \gamma_r + \delta\gamma$, where γ_r is determined from

$$\frac{(1 + a_w^2)}{2\gamma_r^2} = \frac{k_w + k_s}{\omega} - 1 \approx \frac{k_w}{k_s},$$

we obtain ($\delta\gamma \ll \gamma_r$)

$$\begin{aligned} \frac{d\psi}{dz} &= \frac{\omega\,(1 + a_w^2)}{\gamma_r^3}\delta\gamma, \\ \frac{d\delta\gamma}{dz} &= -\frac{d\gamma_r}{dz} - \frac{a_w a_s \omega}{\gamma_r}\sin(\psi + \xi), \end{aligned}$$

and hence the nonlinear pendulum equation[22]:

$$\frac{d^2\psi}{dz^2} = -\frac{\omega^2 a_w a_s\,(1 + a_w^2)}{\gamma_r^4}\sin(\psi + \xi) - \frac{\omega\,(1 + a_w^2)}{\gamma_r^3}\frac{d\gamma_r}{dz}. \tag{5}$$

$d\gamma_r/dz \neq 0$ implies a tapered wiggler in which γ_r varies along the wiggler. It can also represent an external accelerator enhancing the energy of the electron beam.

The electron equations of motion can be written as follows:

$$\frac{d^2\psi}{dz^2} = -\Omega_0^2\frac{a_s}{a_0}\sin(\psi + \xi) + \Omega_0^2 \sin\psi_r, \tag{6}$$

where the synchrotron frequency Ω_0 is defined by

$$\Omega_0^2 \equiv \frac{\omega^2 a_w a_0\,(1 + a_w^2)}{\gamma_r^4} \tag{7}$$

and

$$\Omega_0^2 \sin\psi_r \equiv -\frac{\omega\,(1 + a_w^2)}{\gamma_r^3}\frac{d\gamma_r}{dz}. \tag{8}$$

a_0 is a reference amplitude for the radiation field. In our subsequent analysis, we will consider ψ_r to be constant.

B. Field equations

For the radiation field we use Maxwell's equations

$$\frac{\partial^2 \mathbf{a}_s}{\partial t^2} - \frac{\partial^2 \mathbf{a}_s}{\partial z^2} + k_\perp^2 \mathbf{a}_s = 4\pi \mathbf{j}\frac{e}{mc^2}. \tag{9}$$

Here we are supposing a transverse spatial dependence $\cos k_\perp y$ for all modes. For a waveguided case $\mathbf{a}_s$ must vanish at the wall. We rewrite the x component of the left-hand side of the equation using the form $\mathbf{a}_s \cdot \hat{x} = a\cos(\omega t - k_s z - \xi)$:

$$\left\{\left[\frac{\partial^2 a}{\partial t^2} - \frac{\partial^2 a}{\partial z^2}\right] + \left[-\omega^2 + \left(k^2 + k_\perp^2\right) + 2\omega\dot{\xi} - \dot{\xi}^2 + 2k\xi' + \xi'^2\right] a\right\}\cos(\omega t - k_s z - \xi)$$

$$+ \left\{-2\frac{\partial a}{\partial t}(\omega - \dot{\xi}) - 2\frac{\partial a}{\partial z}(k + \xi') + (\ddot{\xi} - \xi'')a\right\}\sin(\omega t - k_s z - \xi) = 4\pi j_x \frac{e}{mc^2}, \qquad (10)$$

where $\dot{\xi} = \partial\xi/\partial t$, $\xi' = \partial\xi/\partial z$, and we have dropped the subscript s from the amplitude $a_s \to a$. For the current we note that the electron transverse velocity is $-\frac{eA_w}{m\gamma}\cos k_w z$ and the electron density varying as $e^{i\omega t}$ is given by

$$n_0 e^{-i\omega t + i(k_w + k_s)z + i\pi} \oint \frac{d\Gamma}{2\pi} f(\psi, \psi', z) e^{-i\psi}. \qquad (11)$$

Here, n_0 is the incident beam density of electrons multiplied by a "filling factor" of roughly the square of the ratio of the beam radius to the guide radius, f is the distribution function in the phase space Γ where $d\Gamma = d\psi\, d\psi'$ and $\psi' = d\psi/dz$. Thus the electron current is

$$\frac{e}{mc^2} j_x = \frac{e^2 a_w}{m\gamma} n_0 \left[\cos(\omega t - k_s z - \xi)\,\overline{\cos(\psi + \xi)} - \sin(\omega t - k_s z - \xi)\,\overline{\sin(\psi + \xi)}\right], \qquad (12)$$

where we have neglected a nonresonant term $\omega t - (k_s + 2k_w)\, z - \xi$, and the bars indicate a distribution function average. Matching coefficients of $\cos(\omega t - k_s z - \xi)$ and $\sin(\omega t - k_s z - \xi)$ we find

$$\left[\frac{\partial^2 a}{\partial t^2} - \frac{\partial^2 a}{\partial z^2}\right] + \left[-\omega^2 + \left(k_s^2 + k_\perp^2\right) + 2\omega\dot{\xi} + 2k_s\xi' - \dot{\xi}^2 + \xi'^2\right] a$$

$$= \frac{4\pi n_0 e^2 a_w}{m\gamma}\overline{\cos(\psi + \xi)} \qquad (13a)$$

$$\left[\ddot{\xi} - \xi''\right] a - 2(\omega - \dot{\xi})\frac{\partial a}{\partial t} - 2\left(k_s + \xi'\right)\frac{\partial a}{\partial z} = -\frac{4\pi n_0 e^2 a_w}{m\gamma}\overline{\sin(\psi + \xi)}. \qquad (13b)$$

The y component of Maxwell's equations is identical (with the chosen polarization).

We first look for a steady state in which the signal amplitude and phase are constants denoted by a_0 and ξ_0, respectively. This requires us to choose

$$\omega^2 = k_s^2 + k_\perp^2 - \frac{4\pi n_0 e^2 a_w}{m\gamma a_0} C, \tag{14}$$

where

$$C \equiv \overline{\cos(\psi+\xi)_0} \equiv \frac{1}{2\pi}\int d\Gamma\, f_0 \cos(\psi+\xi_0) \tag{15}$$

and f_0 is the steady state electron distribution function.

In order to discuss a steady state in which signal growth in a tapered wiggler ($\overline{\sin(\psi+\xi)_0} \equiv S \equiv \sin\psi_r \neq 0$) is balanced by wave attenuation (which could be produced if part of the signal were being fed off from the waveguide as in an accelerator), we add to the left-hand side of Eq. (13b) a term

$$-\frac{4\pi n_0 e^2}{m\gamma} a_w \frac{a}{a_0} \overline{\sin(\psi+\xi)_0}.$$

Thus, what we are calculating in effect will be the gain of unstable perturbations relative to signal growth. The linearized equations for the perturbed amplitude a_1, and phase $\tilde{\xi}$ are

$$\frac{\partial\tilde{\xi}}{\partial t} + V_g\frac{\partial\tilde{\xi}}{\partial z} + \frac{1}{2\omega}\left(\frac{\partial^2}{\partial t^2} - \frac{\partial^2}{\partial z^2}\right)\tilde{a} + \eta\tilde{a}C = \overline{\eta\cos(\psi+\xi)_1}, \tag{16a}$$

$$\frac{\partial\tilde{a}}{\partial t} + V_g\frac{\partial\tilde{a}}{\partial z} - \frac{1}{2\omega}\left(\frac{\partial^2}{\partial t^2} - \frac{\partial^2}{\partial z^2}\right)\tilde{\xi} + \eta\tilde{a}S = \overline{\eta\sin(\psi+\xi)_1}. \tag{16b}$$

Here,

$$\tilde{a} = \frac{a_1}{a_0}, \qquad V_g = \frac{k_s}{\omega}, \qquad \eta = \frac{2\pi n_0 e^2 a_w}{m\gamma\omega a_0}.$$

Ordinarily, since we are interested in slowly varying terms, the second derivatives could be neglected. However, when the group velocity V_g is close to the electron longitudinal beam velocity $V = \frac{1}{1+(1+a_w^2)/2\gamma_r^2}$, we must retain them. Also note that in deriving the perturbed electron equations we want to use the unperturbed coordinates as variables, hence

$$\overline{\cos(\psi+\xi)_1} = \frac{1}{2\pi}\int \tilde{f}_1 d\Gamma \cos(\psi+\xi_0) - S\tilde{\xi}$$

$$\overline{\sin(\psi+\xi)_1} = \frac{1}{2\pi}\int \tilde{f}_1 d\Gamma \sin(\psi+\xi_0) + C\tilde{\xi}.$$

where $\tilde{f}_1$ is the perturbed distribution function.

C. Dispersion relation

From the electron equations we see that we can define an electron Hamiltonian with $p = d\psi/dz = \partial H/\partial p$, $dp/dz = -\partial H/\partial \psi$:

$$H = \frac{p^2}{2} - \Omega_0^2 \frac{a}{a_0} \cos(\psi + \xi) - \Omega_0^2 \psi \sin \psi_r. \tag{17}$$

We may write this in perturbation form

$$H = H_0 + H_1 \tag{18}$$

with

$$H_0 = \frac{p^2}{2} - \Omega_0^2 \cos(\psi + \xi_0) - \psi \Omega_0^2 \sin \psi_r \tag{19}$$

depending on the equilibrium radiation fields, and

$$H_1 = -\Omega_0^2 \tilde{a} \cos(\psi + \xi_0) + \Omega_0^2 \tilde{\xi} \sin(\psi + \xi_0) \tag{20}$$

which depends on the linear perturbations.

The form of the equilibrium ponderomotive potential well $V_p(\psi)$:

$$V_p(\psi) = -\Omega_0^2 \cos(\psi + \xi_0) - \psi \Omega_0^2 \sin \psi_r$$

is shown in Fig. 1. The bottom of the well is at $\psi = \psi_r$ (modulo 2π), while the top is indicated by the dashed line.

We introduce the action-angle coordinates J and ϕ defined for the steady state Hamiltonian H_0:

$$J = \frac{1}{\pi} \int_{\psi \min}^{\psi \max} \sqrt{2(H_0 - V_p)} d\psi \tag{21}$$

and

$$\phi = \Omega \int^{\psi} \frac{d\psi}{\sqrt{2\left(H_0 - V_p\right)}}, \tag{22}$$

where the synchrotron frequency

$$\Omega = 2\pi \left[2 \int_{\psi\,\mathrm{min}}^{\psi\,\mathrm{max}} \frac{d\psi}{\sqrt{2\left(H_0 - V_p\right)}} \right]^{-1} = \left(\frac{\partial J}{\partial H_0} \right)^{-1}.$$

The steady state Hamiltonian may be expressed as $H_0 = \int^J \Omega(J) dJ$. The element of phase space area $d\Gamma$ is $d\Gamma = dJ\, d\phi$.

An electron orbit in the unperturbed ponderomotive well consists of motion along a horizontal line of fixed J with ϕ increasing as Ωz. Electrons trapped in the well are bounded in ψ. Untrapped electrons are unbounded in ψ, and in a tapered wiggler, they lie progressively further and further away from the tops of the wells as they move down the wiggler. For a long wiggler the untrapped electrons would soon become decoupled from the optical pulse. Under these circumstances, the coupling of sideband modes is due mainly to the trapped electrons. We will therefore not include the untrapped electrons in our discussion. It would require only minor modifications to incorporate them.

Note that if we take $\phi = 0$ as a point in the orbit with vanishing velocity, ψ is an even function of ϕ.

We assume (appropriate for a long wiggler) a phase-mixed equilibrium distribution function for the trapped electrons, i.e., $\partial f_0 / \partial \phi = 0$. Hence, the equilibrium is specified by $f_0(J)$ which we normalize such that $\int f_0(J) dJ = 1$.

The perturbed field variables, $\tilde{a}$ and $\tilde{\xi}$, are assumed to vary as

$$\tilde{a} \rightarrow \tilde{a} e^{i(\lambda\tau - \kappa z)}$$

$$\tilde{\xi} \rightarrow \tilde{\xi} e^{i(\lambda\tau - \kappa z)},$$

where $\lambda\tau \equiv \lambda(t - z/V)$. Note that τ is constant along an electron trajectory. Such perturbations correspond to perturbed radiation fields δa_s

$$\delta a_s \rightarrow a_0 e^{i(\lambda\tau - \kappa z)} \left\{ \tilde{a} \cos\left(\omega t - k_s z - \xi_0\right) + \tilde{\xi} \sin\left(\omega t - k_s z - \xi_0\right) \right\}$$

with components at the sideband frequencies $\omega+\lambda$ and $\omega-\lambda$. We are interested in sideband frequencies close to the signal frequency ω, that is, $\lambda \ll \omega$. We look for solutions of the linearized perturbed equations which are proportional to $e^{i(\lambda\tau-\kappa z)}$. The perturbed distribution function $\tilde{f}_1(J,\phi,z)$ is determined by the linearized Liouville equation

$$\frac{\partial \tilde{f}_1}{\partial z} + \left[\tilde{f}_1, H_0\right] + [f_0, H_1] = 0. \tag{23}$$

The Poisson bracket is defined with respect to the canonical variables J and ϕ,

$$[f,g] = \frac{\partial f}{\partial \phi}\frac{\partial g}{\partial J} - \frac{\partial f}{\partial J}\frac{\partial g}{\partial \phi}.$$

The perturbed Hamiltonian H_1 is

$$H_1 = -\Omega_0^2\left\{\tilde{a}\cos(\psi+\xi_0) - \tilde{\xi}\sin(\psi+\xi_0)\right\}e^{-i\kappa z}, \tag{24}$$

where $\lambda(t-z/V)-\kappa z = \lambda\pi/\omega - \lambda\psi(J,\phi)/\omega - \kappa z \approx -\kappa z$, and the equilibrium quantities $\cos(\psi+\xi_0)$, $\sin(\psi+\xi_0)$ may be expressed as a Fourier series in ϕ

$$\cos(\psi+\xi_0) = \sum \alpha_m(J)e^{im\phi}, \qquad \sin(\psi+\xi_0) = \sum \beta_m e^{im\phi}.$$

Thus, for $\tilde{f}_1 = f_1 e^{-i\kappa z}$, we obtain

$$f_1 = \sum e^{im\phi}\frac{\Omega_0^2 m}{\kappa - m\Omega}\left[\tilde{a}\alpha_m - \tilde{\xi}\beta_m\right]\frac{\partial f_0}{\partial J}. \tag{25}$$

Hence we find

$$\begin{aligned}
\overline{\cos(\psi+\xi)_1} &= \tilde{a}\left[\int \sum \frac{m\Omega_0^2}{\kappa - m\Omega}\alpha_m\alpha_{-m}\frac{\partial f_0}{\partial J}dJ\right] \\
&- \tilde{\xi}\left[S + \int \frac{\partial f_0}{\partial J}dJ \sum \frac{m\Omega_0^2}{\kappa - m\Omega}\beta_m\alpha_{-m}\right] \qquad (26) \\
\overline{\sin(\psi+\xi)_1} &= \tilde{a}\left[\int \sum \frac{m\Omega_0^2}{\kappa - m\Omega}\alpha_m\beta_{-m}\frac{\partial f_0}{\partial J}dJ\right] \\
&+ \tilde{\xi}\left\{C - \int \sum \frac{m\Omega_0^2}{\kappa - m\Omega}\beta_m\beta_{-m}\frac{\partial f_0}{\partial J}dJ\right\}. \qquad (27)
\end{aligned}$$

We may note further that from the symmetries of the potential $\alpha_m = \alpha_{-m}$, $\beta_m = \beta_{-m}$ and hence α_m, β_m are real.

To complete the formal solution to our problem we return to the linearized equations for the fields. The assumed time and space dependence of the perturbed fields are $e^{i(\lambda\tau - \kappa z)}$, and thus a positive imaginary part of κ indicates growth for real λ of coupled sideband modes at frequencies $(\omega + \lambda, \omega - \lambda)$. From Eq. (16) we obtain the following pair of equations to determine $\kappa(\lambda)$:

$$\left[-i\kappa + i\lambda\left(1 - \frac{V_g}{V}\right) + \eta S\right]\tilde{\xi} + \left[\frac{\lambda^2}{\omega}\left(\frac{1}{V} - 1\right) + \frac{\lambda}{\omega}\frac{\kappa}{V} + \eta C\right]\tilde{a} = \eta\tilde{a}I_1 - \eta\tilde{\xi}I_2 \quad (28a)$$

$$\left[-i\kappa + i\lambda\left(1 - \frac{V_g}{V}\right) + \eta S\right]\tilde{a} - \left[\frac{\lambda^2}{\omega}\left(\frac{1}{V} - 1\right) + \frac{\lambda}{\omega}\frac{\kappa}{V} + \eta C\right]\tilde{\xi} = \eta\tilde{a}I_3 - \eta\tilde{\xi}I_4, \quad (28b)$$

where

$$I_1 = \int\sum \frac{m\Omega_0^2}{\kappa - m\Omega}\alpha_m\alpha_{-m}\frac{\partial f_0}{\partial J}dJ \quad (29)$$

$$I_2 = \int\sum \frac{m\Omega_0^2}{\kappa - m\Omega}\beta_m\alpha_{-m}\frac{\partial f_0}{\partial J}dJ = I_3 \quad (30)$$

$$I_4 = \int\sum \frac{m\Omega_0^2}{\kappa - m\Omega}\beta_m\beta_{-m}\frac{\partial f_0}{\partial J}dJ. \quad (31)$$

The I's all depend on κ, but not λ. We have approximated

$$\frac{\partial^2}{\partial t^2} - \frac{\partial^2}{\partial z^2} = \left(\frac{\partial}{\partial t} + \frac{\partial}{\partial z}\right)\left(\frac{\partial}{\partial t} - \frac{\partial}{\partial z}\right) \approx 2\frac{\partial}{\partial t}\left(\frac{\partial}{\partial t} + \frac{\partial}{\partial z}\right)$$

to eliminate unphysical backward waves. We denote $(\lambda/\omega)\left(\lambda\left(\frac{1}{V} - 1\right) + \kappa\right) \equiv \tilde{\lambda}^2$. The form of $\tilde{\lambda}^2$ will depend on just what phenomenon is reducing the wave group velocity. Here we have assumed it is due to waveguiding. Our dispersion relation is thus

$$D(\kappa) = \left[\kappa - \lambda\left(1 - \frac{V_g}{V}\right)\right]^2 + 2i\left[\kappa - \lambda\left(1 - \frac{V_g}{V}\right)\right]\eta S - \eta^2\left(S^2 - I_2^2\right) - \left(\tilde{\lambda}^2 + \eta C - \eta I_1\right)\left(\tilde{\lambda}^2 + \eta C - \eta I_4\right) = 0. \quad (32)$$

A solution for κ with positive imaginary part for real λ corresponds to instability.

We analyze this dispersion relation in Sec. III for the limit of electrons trapped at the bottom of the well and in Sec. IV for arbitrary trapped electron distribution functions.

For convenience, we summarize below the symbols used throughout the text of this paper.

ω	signal frequency
k_s	signal wavenumber
A_s	signal vector potential amplitude
$a_s \equiv eA_s/mc^2 = a$	
ξ	signal phase
$\alpha_c = a\cos\xi$	
$\alpha_s = a\sin\xi$	
$a_0,\ \xi_0$	steady state signal amplitude and phase
V_g	signal group velocity
k_w	wiggler wavenumber
A_w	wiggler vector potential amplitude
$a_w \equiv eA_w/mc^2$	
L	wiggler length
V	longitudinal electron beam velocity
$\gamma = E/mc^2$	electron beam energy
$\psi = (k_w + k_s)\,z - \omega t + \pi$	optical phase
$\psi' = d\psi/dz$	
$\gamma_r = (k_s/2k_w)^{1/2}\,(1 + a_w^2)^{1/2}$	resonant energy
n_0	beam electron density
$\eta = \frac{2\pi n_0 e^2 a_w}{m\gamma\omega a_0}$	scaled current density
$J,\ \phi\ dJ\,d\phi = d\psi\,d\psi'$	action-angle variables of electrons trapped in ponderomotive well
Ω	synchrotron frequency
$\Omega_0 = \frac{\omega\left(1+a_w^2\right)^{1/2}}{\gamma_r^2}\,(a_w a_0)^{1/2}$	synchrotron frequency at bottom of the well
$f_0(J)$	steady state electron distribution function
$C = \int \frac{dJ\,d\phi}{2\pi} f_0 \cos(\psi + \xi_0)$	
$S = \int \frac{dJ\,d\phi}{2\pi} f_0 \sin(\psi + \xi_0) = \sin\psi_r$	
$\omega - \lambda,\ \omega + \lambda$	frequencies of sideband modes
κ	wavenumber of sideband modes
$\mathrm{Im}\,\kappa$	spatial growth rate of sideband modes
$\tilde{\lambda}^2 = \lambda\left(\lambda(1/V - 1) + \kappa\right)/\omega$	
$\tilde{a}$	perturbed radiation amplitude
$\tilde{\xi}$	perturbed radiation phase
H	Hamiltonian for electron motion
$D\left(\kappa(\lambda)\right)$	dispersion function for sideband modes
$\overline{\overline{\cos\psi}} = \frac{1}{2\pi}\int d\phi\cos\psi$	average over equilibrium electron orbit
$p = \psi' = \{2\left[H_0 + \Omega_d^3\cos\psi + \psi\sin\psi_r\right]\}$	electron momentum
$Q(J),\ P(J)$	functions determining stability
$E,\ K$	complete elliptic integrals
$\alpha_m \equiv 1/2\pi\overline{\overline{\cos\psi e^{-im\phi}}}$	
$\beta_m = 1/2\pi\overline{\overline{\sin\psi e^{-im\phi}}}$	

III. Bottom of the Well

This dispersion relation simplifies if we assume that all the trapped electrons are at the bottom of the ponderomotive well. In this limit, $f_0(J) = \delta(J)$.

The electron orbits near the bottom of the well may be approximated by the Hamiltonian

$$H_0 \to \frac{p^2}{2} + \Omega_0^2 \frac{(\delta\psi)^2}{2} \cos\psi_r,$$

where

$$\psi + \xi_0 = \psi_r + \delta\psi$$

and we have expanded $\cos(\psi + \xi_0)$ in a Taylor series about the bottom of the well ψ_r.

It may be verified that

$$\delta\psi = \hat{\psi}\cos\phi,$$

where $\hat{\psi}$ is the maximum excursion from the well bottom and the oscillation angle ϕ is determined by

$$\frac{d\phi}{dz} = \Omega \equiv \Omega_0 (\cos\psi_r)^{1/2}.$$

Furthermore,

$$\begin{aligned}
J &= \frac{\Omega\hat{\psi}^2}{2} \\
\alpha_1 &= \alpha_{-1} = -\sin\psi_r \frac{\tilde{\psi}}{2} \\
\beta_1 &= \beta_{-1} = \cos\psi_r \frac{\tilde{\psi}}{2} \\
I_1 &= -\frac{\sin^2\psi_r \Omega_0^2}{\kappa^2 - \Omega^2} \\
I_2 &= \frac{\sin\psi_r \cos\psi_r \Omega_0^2}{\kappa^2 - \Omega^2} = I_3 \\
I_4 &= -\frac{\cos^2\psi_r \Omega_0^2}{\kappa^2 - \Omega^2} \\
S &= \sin\psi_r \\
C &= \cos\psi_r.
\end{aligned}$$

Substituting in Eq. (32), we obtain the dispersion relation

$$D(\kappa) = \left[\kappa - \lambda\left(1 - \frac{V_g}{V}\right)\right]^2 + 2i\eta S\left[\kappa - \lambda\left(1 - \frac{V_g}{V}\right)\right] - \tilde{\lambda}^4 - 2\tilde{\lambda}^2\eta C - \eta^2 - \frac{\eta\Omega^2}{C}\frac{\left(\tilde{\lambda}^2 + \eta C\right)}{(\kappa^2 - \Omega^2)}. \quad (33)$$

A. Untapered wiggler

We will first analyze the case of an untapered wiggler where $S = 0$. The dispersion relation may be written as follows:

$$D(\kappa) = Y_1(\kappa) - Y_2(\kappa), \quad (34)$$

where

$$Y_1(\kappa) = \left(1 - \frac{\lambda^2}{\omega^2}\right)\left(\kappa^2 - 2\kappa b_1\right) + b_2$$

$$= \left(1 - \frac{\lambda^2}{\omega^2}\right)\left[(\kappa - b_1)^2 - d_0^2\right] \quad (35)$$

$$Y_2(\kappa) = \frac{d_1\left(\kappa + d_2\right)}{(\kappa^2 - \Omega^2)} \quad (36)$$

$$b_1 \equiv \frac{1}{(1 - \lambda^2/\omega^2)}\left[\lambda\left(1 - \frac{V_g}{V}\right) + \frac{\lambda}{\omega}\eta + \frac{\lambda^3}{\omega^2}\left(\frac{1}{V} - 1\right)\right]$$

$$b_2 \equiv \lambda^2\left(1 - \frac{V_g}{V}\right)^2 - \left[\eta + \frac{\lambda^2}{\omega}\left(\frac{1}{V} - 1\right)\right]^2$$

$$d_0^2 = b_1^2 - \frac{b_2}{(1 - \lambda^2/\omega^2)}$$

$$= \frac{1}{(1 - \lambda^2/\omega^2)^2}\left[\eta + \frac{\lambda^2}{\omega V}\left(1 - V_g\right)\right]^2$$

$$d_1 \equiv \frac{\lambda\eta\Omega^2}{\omega} > 0$$

$$d_2 \equiv \frac{\omega\eta}{\lambda} + \lambda\left(\frac{1}{V} - 1\right) > 0.$$

Hereafter, we consider λ and ω to be positive without loss of generality, and $\lambda \ll \omega$ since we are interested in sideband frequencies close to the signal frequency ω.

In Fig. 2 and Fig. 3, $Y_1(\kappa)$ and $Y_2(\kappa)$ are plotted schematically as a function of κ. $D(\kappa) = 0$ at those values of κ where the curves $Y_1(\kappa)$ and $Y_2(\kappa)$ intersect.

$Y_1(\kappa) = b_2$ at $\kappa = 0$, $Y_1(\kappa) = 0$ at $\kappa = b_1 \pm d_0$, and $Y_1(\kappa)$ is a minimum equal to $-(1-\lambda^2/\omega^2)\, d_0^2$ at $\kappa = b_1$. If $b_2 < 0$, $b_1 - d_0 < 0$ and $b_1 + d_0 > 0$.

$Y_2(\kappa) = -\frac{d_1 d_2}{\Omega^2}$ at $\kappa = 0$, $Y_2(\kappa) = 0$ at $\kappa = -d_2$, and $Y_2(\kappa)$ has poles at $\kappa^2 = \Omega^2$.

It may readily be verified from Fig. 2 and Fig. 3 that there exists four real roots of $D(\kappa) = 0$ if

$$\begin{aligned} b_2 &< -\frac{d_1 d_2}{\Omega_2} \\ b_1 - d_0 &> -d_2. \end{aligned}$$

The second inequality is always satisfied ($\lambda < \omega$), and the first inequality is satisfied if

$$\left(1 - \frac{V_g}{V}\right)^2 < \frac{\eta}{\omega}\left(\frac{1}{V} - 1\right). \tag{37}$$

Equation (37) constitutes a sufficient condition for stability.

1. Linear growth rates

In order to obtain an estimate of the unstable growth rates, we assume that Eq. (37) is strongly violated. We look for solutions where

$$\kappa \sim \lambda\left(1 - \frac{V_g}{V}\right) \sim \lambda\left(\frac{1}{V} - 1\right) \lesssim \Omega.$$

Let $\kappa = \lambda\,(1 - V_g/V) + \delta$, where $\delta < |\lambda\,(1 - V_g/V)|$.

If $\lambda\,(1 - V_g/V) = \Omega$, the equation for δ, obtained from Eq. (33), may be approximated by

$$\delta^3 - \delta\left[\eta + \frac{\Omega^2\,(1 - V_g)}{\omega V\,(1 - V_g/V)^2}\right]^2 - \frac{\eta\Omega}{2}\left[\eta + \frac{\Omega^2\,(1 - V_g)}{\omega V\,(1 - V_g/V)^2}\right] = 0. \tag{38}$$

There exists a pair of complex conjugate roots when

$$1 > \frac{16}{27}\frac{\eta^2}{\Omega^2}\left\{1 + \frac{\Omega^2\left(1 - V_g\right)}{\eta\omega V\left(1 - V_g/V\right)^2}\right\}^4.$$

For

$$\frac{\Omega^2\left(1 - V_g\right)}{\eta\omega V\left(1 - V_g/V\right)^2} \ll 1,$$

the unstable sideband growth rate is

$$\mathrm{Im}(\kappa) = \mathrm{Im}(\delta) \approx \frac{(3)^{1/2}}{2}\left(\frac{\eta^2\Omega}{2}\right)^{1/3}. \tag{39}$$

If $\lambda\left(1 - V_g/V\right) \ll \Omega$, the equation for δ may be approximated by

$$\delta^2 + \lambda^2\left[\frac{\eta\left(1 - V_g/V\right)^2}{\Omega^2} - \frac{\left(1 - V_g\right)}{\omega V}\right]\left[\eta + \frac{\lambda^2}{\omega V}\left(1 - V_g\right)\right] = 0 \tag{40}$$

and the sideband is unstable if

$$\frac{\eta\left(1 - V_g/V\right)^2}{\Omega^2} > \frac{\left(1 - V_g\right)}{\omega V}.$$

B. Tapered wiggler

In the case of a tapered wiggler ($S \neq 0$), we perform a Nyquist analysis to determine if there are unstable roots of the dispersion relation with $\mathrm{Im}(\kappa) > 0$. It is useful to define a new function $G(\kappa)$ which is well behaved at infinity

$$G(\kappa) = \frac{F(\kappa)}{\left(\kappa^4 + \Lambda^2\right)}, \tag{41}$$

where $F(\kappa) = \left(\kappa^2 - \Omega^2\right)D(\kappa)$, and Λ^2 is a large, real, positive constant. $F(\kappa)$ has no poles. $G(\kappa)$ has two poles in the upper half of the κ-plane.

When $\mathrm{Re}(\kappa) \to \pm\infty$, $G \to \left(1 - \lambda^2/\omega^2\right) + \frac{2i\eta S}{\kappa}$. On the real axis ($\mathrm{Im}(\kappa) = 0$), the imaginary part of G vanishes for $\kappa = \pm\Omega$ and $\kappa = \lambda\left(1 - V_g/V\right)$. Let us denote the magnitude of $\mathrm{Re}(F)$ at these values of κ by

$$R(a) \equiv \mathrm{Re}(F)_{\kappa=-\Omega}$$

$$= -\frac{\eta\Omega^2}{C}\left\{\eta C + \frac{\lambda}{\omega}\left[\lambda\left(\frac{1}{V}-1\right)-\Omega\right]\right\} \tag{42}$$

$$\begin{aligned} R(b) &\equiv \mathrm{Re}(F)_{\kappa=\lambda(1-V_g/V)} \\ &= -\left[\lambda^2\left(1-\frac{V_g}{V}\right)^2-\Omega^2\right]\frac{\lambda^2}{\omega V}(1-V_g)\left[\frac{\lambda^2}{\omega V}(1-V_g)+\eta C\left(1-\frac{S^2}{C^2}\right)\right] \\ &\quad -\lambda^2\left(1-\frac{V_g}{V}\right)^2\left[\eta^2+\frac{\eta\lambda^2}{\omega V C}(1-V_g)\right] \end{aligned} \tag{43}$$

$$\begin{aligned} R(c) &= \mathrm{Re}(F)_{\kappa=\Omega} \\ &= -\frac{\eta\Omega^2}{C}\left\{\eta C + \frac{\lambda}{\omega}\left[\lambda\left(\frac{1}{V}-1\right)+\Omega\right]\right\} < 0. \end{aligned} \tag{44}$$

Let us consider the range of λ satisfying $|\lambda(1-V_g/V)| < \Omega$. Then as κ moves on a contour along the real axis from $\kappa = -\infty$ to $\kappa = +\infty$, $G(\kappa)$ moves along the contour shown in Fig. 4. If $R(a) < 0$, $R(b) > 0$, $R(c) < 0$, the contour encircles the origin twice in the clockwise direction. $G(\kappa)$ has two poles and no zeros in the upper half of the κ-plane. Thus, $F(\kappa)$ (and hence $D(\kappa)$) has no unstable roots.

Similarly, $F(\kappa)$ has no unstable roots for $\lambda(1-V_g/V) < -\Omega$ if $R(a) > 0$, $R(b) < 0$, $R(c) < 0$, and for $\lambda(1-V_g/V) > \Omega$ if $R(a) < 0$, $R(b) < 0$, $R(c) > 0$.

Since $R(c)$ is negative definite, $F(\kappa)$ has at least one unstable root when $\lambda(1-V_g/V) > \Omega$, and a necessary but not sufficient condition for stability is $(1-V_g/V) = 0$.

If $1-V_g/V = 0$, the additional requirements for stability are ($R(a) < 0$, $R(b) > 0$):

$$\begin{aligned} \frac{\lambda}{\omega}\left\{\Omega-\lambda\left(\frac{1}{V}-1\right)\right\}-\eta C &< 0 \\ \frac{\lambda^2}{\omega}\left(\frac{1}{V}-1\right)+\eta C\left(1-\frac{S^2}{C^2}\right) &> 0. \end{aligned}$$

These inequalities can be satisfied if $4\eta C\omega\left(\frac{1}{V}-1\right) > \Omega^2$, $C^2 - S^2 > 0$.

Thus, the necessary and sufficient conditions for $F(\kappa)$ and hence $D(\kappa)$ to have no unstable roots are

$$1-\frac{V_g}{V} = 0 \tag{45a}$$

$$4\eta C\omega\left(\frac{1}{V}-1\right) > \Omega^2 \tag{45b}$$

$$C^2 > S^2. \tag{45c}$$

If any one of these criteria is not satisfied, $F(\kappa)$ will have an unstable root.

1. Linear growth rate

In the following discussion, we estimate the magnitude of the unstable growth rates. We focus on those sideband modes which are unstable because S is finite.

1) $\lambda^2\left(1-V_g/V\right)^2 < \Omega^2$.

In the range $\lambda^2\left(1-V_g/V\right)^2 < \Omega^2$, there may be a low mode number instability with $\kappa^2 \ll \Omega^2$ or a high mode number instability with $\kappa^2 \sim \Omega^2$.

Let us look for solutions $\kappa = \lambda\left(1-V_g/V\right)+\delta$, where $|\lambda\left(1-V_g/V\right)| > |\delta|$. The dispersion relation (Eq. (33)) may then be approximated by

$$(\delta + i\eta S)^2 = -\eta^2 S^2 + \frac{R(b)}{\Omega^2 - \lambda^2\left(1-V_g/V\right)^2}, \tag{46}$$

where

$$\begin{aligned}\frac{R(b)}{\Omega^2-\lambda^2\left(1-V_g/V\right)^2} \approx & -\frac{\lambda^2\left(1-V_g/V\right)^2}{\Omega^2}\eta\left[\eta+\frac{\lambda^2}{\omega VC}\left(1-V_g\right)\right] \\ & -\frac{\lambda^2\left(1-V_g\right)}{\omega V}\left[\left(\frac{S^2}{C^2}-1\right)\eta-\frac{\lambda^2}{\omega V}\left(1-V_g\right)\right].\end{aligned}$$

ηS is the main signal gain produced by wiggler tapering. If $R(b) < 0$, the sideband gain will exceed the signal gain.

Thus, a low mode number instability occurs when

$$\frac{\eta\omega}{\Omega^2}\left(1-\frac{V_g}{V}\right)^2 > \frac{\left(1-V_g\right)}{V}.$$

For $S \to 0$, $C \to 1$, we recover the growth rate previously derived for an untapered wiggler.

For

$$\frac{\eta\omega\left(1-V_g/V\right)^2}{\Omega^2} < \frac{(1-V_g)}{V},$$

the instability occurs in the range

$$\eta C\left(\frac{S^2}{C^2}-1\right) > \frac{\lambda^2}{\omega V}(1-V_g)$$

which will only be possible for $S^2 > C^2$. The growth rate at the optimal value of

$$\frac{\lambda^2}{\omega V}(1-V_g) = \frac{\eta C}{2}\left(\frac{S^2}{C^2}-1\right)$$

is

$$\begin{aligned}\delta &= \frac{i\eta}{2C} - i\eta S \\ &= \frac{i\eta C}{2}\left(\frac{S}{C}-1\right)^2. \end{aligned} \tag{47}$$

For validity, we require

$$\Omega^2 > \frac{\eta\omega VC}{2}\left(\frac{S^2}{C^2}-1\right)\frac{\left(1-V_g/V\right)^2}{(1-V_g)} > \frac{\eta^2C^2}{4}\left(\frac{S}{C}-1\right)^4.$$

The high mode number instability occurs when $(R(a) > 0)$

$$\frac{1}{4\left(1/V-1\right)^2}\left\{\Omega^2 - 4\eta C\omega\left(\frac{1}{V}-1\right)\right\} - \left\{\lambda - \frac{\Omega}{2\left(1/V-1\right)}\right\}^2 > 0.$$

This will only be possible for $\Omega^2 > 4C\eta\omega\left(1/V-1\right)$. Assuming this inequality is satisfied and taking

$$\lambda = \frac{\Omega}{2\left(1/V-1\right)},$$

we look for solutions $\kappa = -\Omega + \delta$, where $\Omega \gg \delta$. The dispersion relation may then be approximated by

$$-2\Omega\delta + \frac{R(a)}{\Omega^2 - i2\eta S\Omega} = 0 \tag{48}$$

and the unstable growth rate is given by

$$\delta = \frac{\eta\Omega}{8\omega\left(1/V-1\right)C}\frac{\left[1+\frac{2i\eta S}{\Omega}\right]}{\left[1+\frac{4\eta^2S^2}{\Omega^2}\right]}. \tag{49}$$

For validity, we require ($\Omega > |\delta|$)

$$1 > \frac{\eta}{8\omega\,(1/V-1)\,C}$$

and $\left(\lambda^2\,(1-V_g/V)^2 < \Omega^2\right)$

$$1 > \frac{(1-V_g/V)^2}{4\,(1/V-1)^2}.$$

2) The case $4\eta C\omega(1/V-1) > \Omega^2$.

We now assume that conditions 45b) and 45c) are satisfied and look for the consequences of not exactly matching the non-slippage condition 45a). In this case as we have seen there should be one unstable root if $\left|\lambda\left(1-\frac{V_g}{V}\right)\right| > \Omega$ and none if $\left|\lambda\left(1-\frac{V_g}{V}\right)\right| < \Omega$.

We may write Eq. (33) in the form

$$\left(\kappa^2-\Omega^2\right)\left[\left(\kappa-\lambda\left(1-\frac{V_g}{V}\right)+i\eta S\right)^2-\left(\tilde{\lambda}^2+\eta c\right)^2\right]=\frac{\eta\Omega^2}{c}\left(\tilde{\lambda}^2+\eta c\right).$$

We look for the root near $\kappa = \pm\Omega$ and find

$$\kappa=\pm\Omega\left[1+\frac{\eta\tilde{\tilde{\lambda}}^2/2}{\left[\pm\Omega-\lambda\left(1-\frac{V_g}{V}\right)\right]^2-\tilde{\tilde{\lambda}}^4+2i\eta S\left[\pm\Omega-\lambda\left(1-\frac{V_g}{V}\right)\right]}\right], \tag{50}$$

where $\tilde{\tilde{\lambda}}^2 \equiv \tilde{\lambda}^2+\eta c \approx \tilde{\lambda}^2 \approx \frac{\lambda^2}{\omega}\left(\frac{1}{V}-1\right)$ since $\left|\lambda\left(1-\frac{V_g}{V}\right)\right| \sim |\kappa| \ll \left|\lambda\left(\frac{1}{V}-1\right)\right|$. It is clear that an unstable root will occur only if $\left|\lambda\left(1-\frac{V_g}{\Omega}\right)\right| \gtrsim \Omega$.

Further, we define

$$\begin{aligned}\alpha &\equiv \frac{\Omega\left(\frac{1}{V}-1\right)}{\omega\left(1-\frac{V_g}{V}\right)^2}\\ &\approx \frac{2a_w^{1/2}a_0^{1/2}}{\left(1+a_w^2\right)^{1/2}}\frac{\left(\frac{1}{V}-1\right)^2}{\left(1-\frac{V_g}{V}\right)^2},\end{aligned}$$

where we have used Eq. (7) to express α in more physical terms. Then

$$\begin{aligned}\frac{\tilde{\lambda}^2}{\left|\lambda\left(1-\frac{V_g}{V}\right)\right|} &= \frac{\left|\lambda\left(1-\frac{V_g}{V}\right)\right|}{\omega}\frac{\left(\frac{1}{V}-1\right)}{\left(1-\frac{V_g}{V}\right)^2}\\ &\geq \alpha.\end{aligned}$$

We will now assume that $\alpha > 1$, i.e., $\omega\left(1-\frac{V_g}{V}\right)^2 < \Omega\left(\frac{1}{V}-1\right)$ in order to find the low slippage limit. This also implies $\tilde{\lambda}^2 \gg \eta$. In that case Eq. (50) may be expanded to find

$$\kappa = \pm\Omega\left[1-\frac{\eta}{2\tilde{\lambda}^2}\left[1+\frac{2i\eta s}{\tilde{\lambda}^4}\left(\pm\Omega-\lambda\left(1-\frac{V_g}{V}\right)\right)\right]\right].$$

The growth rate is now easily maximized with respect to λ to yield

$$\begin{aligned}\kappa_i = \delta &= \frac{1}{5}\left(\frac{5}{6}\right)\frac{\eta^2 S}{\Omega\alpha^3} \\ &= .06\frac{\eta^2 S}{\Omega\alpha^3} \\ &= .06\frac{\eta^2 S}{\Omega}\left[\frac{\omega^3\left(1-\frac{V_g}{V}\right)^6}{\Omega^3\left(\frac{1}{V}-1\right)^3}\right]. \qquad (51a)\end{aligned}$$

Hence, the growth rate vanishes very rapidly $\sim\left(1-\frac{V_g}{V}\right)^6$ as slippage disappears and we may regard our condition for validity ($\alpha > 1$)

$$\omega\left(1-\frac{V_g}{V}\right)^2 < \Omega\left(\frac{1}{V}-1\right) \qquad (51b)$$

as the effective criterion for a high degree of stabilization.

As slippage increases and α becomes smaller an approximate solution of 50) for the growth rate at worst λ is $\delta = \frac{\eta^2 S}{\Omega\alpha(4\alpha-1)^2}$. As $\alpha \to 1/4$ the expansion breaks down and $\delta \sim (\eta\Omega)^{1/2}$ so that the stabilization completely disappears.

IV. Distribution of Trapped Electrons

In real physical devices, there will be a distribution of electrons trapped in the ponderomotive well. The integrals I_1, I_2, I_3, I_4 depend on the electron distribution function f_0 and in general have no simple closed forms. They are nonsingular, complex functions of κ.

To obtain relatively simple analytic results, we first consider the case of the untapered wiggler where $\sin\psi_r = 0$ and the equilibrium electron orbits can be expressed in terms of elliptic functions. The case of tapered wigglers with $\sin\psi_r \neq 0$ is more complicated, and we

will discuss only the small κ/Ω_0 regime where we are able to expand the dispersion relation as a power series in κ/Ω_0.

A. Untapered wigglers

For untapered wigglers, the action variable J is

$$\begin{aligned} J &= \frac{8\Omega_0}{\pi}\int_0^{\pi/2} d\theta \frac{k^2\cos^2\theta}{\left(1-k^2\sin^2\theta\right)^{1/2}} \\ &= \frac{8\Omega_0}{\pi}\left\{E\left(k^2\right)-\left(1-k^2\right)K\left(k^2\right)\right\}, \end{aligned} \tag{52}$$

where

$$\begin{aligned} k^2 &= \frac{H_0+\Omega_0^2}{2\Omega_0^2}, \\ K\left(k^2\right) &= \int_0^{\pi/2}\frac{d\theta}{\left(1-k^2\sin^2\theta\right)^{1/2}} \\ E\left(k^2\right) &= \int_0^{\pi/2} d\theta\left(1-k^2\sin^2\theta\right)^{1/2}, \end{aligned}$$

K and E are the complete Elliptic Integrals of the first and second kind. Equation (52) implicitly defines $k^2(J)$ and $H_0(J)$.

The electron equilibrium trajectories are expressible in terms of the action-angle variables J and ϕ by

$$\sin\frac{(\psi+\xi_0)}{2} = k\,\mathrm{sn}(u-K), \tag{53}$$

where $d\psi/dz = 0$ at $\phi = 0$, and

$$\frac{d\phi}{dz} = \frac{\partial H_0}{\partial J} = \frac{\pi\Omega_0}{2K\left(k^2\right)} \equiv \Omega, \qquad u = \frac{2K}{\pi}\phi.$$

Thus,

$$\begin{aligned} \cos\left(\psi+\xi_0\right) &= 1-2\sin^2\frac{(\psi+\xi_0)}{2} \\ &= 1-2k^2\,\mathrm{sn}^2(u-K) \end{aligned} \tag{54}$$

$$\begin{aligned}\sin(\psi+\xi_0) &= 2\sin\frac{(\psi+\xi_0)}{2}\cos\frac{(\psi+\xi_0)}{2}\\ &= 2k\,\mathrm{sn}(u-K)\,\mathrm{dn}(u-K)\\ &= -2k\frac{\partial}{\partial u}\,\mathrm{cn}(u-K). \qquad (55)\end{aligned}$$

$\mathrm{sn}\,\chi$, $\mathrm{cn}\,\chi$, $\mathrm{dn}\,\chi$ are the Jacobian elliptic functions defined by[23]

$$\begin{aligned}\mathrm{sn}\,\chi &= \sin\theta\\ \mathrm{cn}\,\chi &= \cos\theta\\ \mathrm{dn}\,\chi &= \left(1-k^2\sin^2\theta\right)^{1/2}\\ \chi &= \int_0^\theta \frac{d\theta'}{\left[1-k^2\sin^2\theta'\right]^{1/2}}.\end{aligned}$$

From the Fourier series expansion of $\mathrm{cn}(u-K)$ and $\mathrm{sn}^2(u-K)$, we obtain for the coefficients α_m and β_m

$$\alpha_m = \frac{1}{2\pi}\oint d\phi\cos(\psi+\xi_0)\,e^{-im\phi} = \begin{cases} 2E/K-1 & m=0\\ \dfrac{(-1)^{m/2}\pi^2 m q^{m/2}}{K^2(1-q^m)} & m \text{ even}\\ 0 & m \text{ odd}\end{cases} \qquad (56)$$

$$\beta_m = \frac{1}{2\pi}\oint d\phi\sin(\psi+\xi_0)\,e^{-im\phi} = \begin{cases} 0 & m \text{ even}\\ \dfrac{(-1)^{(m+1)/2}\pi^2 m q^{m/2}}{K^2(1+q^m)} & m \text{ odd,}\end{cases} \qquad (57)$$

where $q \equiv \exp\left[-\pi K\left(k'^2\right)/K\left(k^2\right)\right]$ and $k'^2 = 1-k^2$.

Furthermore, we obtain for C, S, I_1, I_2, I_3, and I_4

$$C = \frac{1}{2\pi}\int dJ\,f_0\oint\frac{d\psi\cos(\psi+\xi_0)}{[2(H-V)]^{1/2}} = \int dJ\,f_0\left(\frac{2E}{K}-1\right) \qquad (58)$$

$$S = 0$$

$$I_1 = \sum_{m\ \text{even}}\int dJ\frac{\partial f_0}{\partial J}\frac{\pi^4 m^3 q^m\Omega_0^2}{K^4(1-q^m)^2(\kappa-m\Omega)} \qquad (59)$$

$$
\begin{aligned}
I_2 &= 0 = I_3 \\
I_4 &= \sum_{m \text{ odd}} \int \frac{\partial f_0}{\partial J} dJ \frac{\pi^4 m^3 q^m \Omega_0^2}{K^4 (1+q^m)^2 (\kappa - m\Omega)}
\end{aligned} \tag{60}
$$

When $\kappa^2 \ll \Omega^2$, I_1 and I_4 may be approximated by ($\kappa = \kappa_r + i\epsilon$, $\epsilon \to 0$)

$$
I_1 = I_{1r} + I_{1i}
$$

$$
I_4 = I_{4r} + I_{4i},
$$

where

$$
\begin{aligned}
I_{1r} &= -\sum_{\substack{m>0 \\ \text{even}}} \int dJ \frac{\partial f_0}{\partial J} \frac{4\pi^3 m^2 q^m \Omega_0}{K^3 (1-q^m)^2} + \cdots \\
&= \int dJ \frac{\partial f_0}{\partial J} \frac{8\Omega_0}{\pi} \left\{ E\left(\frac{E}{K} - 1\right) + \frac{1}{3}\left(2k^2 E - E + k'^2 K\right) \right\} + \cdots \qquad (61) \\
I_{1i} &= -i\pi \int dJ \frac{\partial f_0}{\partial J} \frac{\pi^4 m^3 q^m \Omega_0^2}{K^4 (1-q^m)^2} \frac{\delta(J - J_0)}{|m\partial\Omega/\partial J|} \\
I_{4r} &= -\sum_{\substack{m>0 \\ \text{odd}}} \int dJ \frac{\partial f_0}{\partial J} \frac{4\pi^3 m^2 q^m \Omega_0}{K^3 (1+q^m)^2} \left\{ 1 + \frac{\kappa^2}{m^2\Omega^2} + \cdots \right\} \\
&= \int dJ\, f_0 \left(\frac{2E}{K} - 1\right) + \frac{\kappa^2}{\Omega_0^2} + \cdots \qquad (62) \\
I_{4i} &= -i\pi \int \frac{\partial f_0}{\partial J} dJ \frac{\pi^4 m^3 q^m \Omega_0^2}{K^4 (1+q^m)^2} \frac{\delta(J - J_0)}{|m\partial\Omega/\partial J|},
\end{aligned}
$$

where J_0 is determined by $m\Omega(J_0) = \kappa$, the condition for "bounce" resonant interactions.

Substitution of the integrals given by Eqs. (59) and (60) into Eq. (32) yields the linear dispersion relation for an untapered wiggler. We now discuss the stability properties to determine if a root exists with complex κ for real λ.

It is again instructive to perform a Nyquist analysis in order to obtain sufficient conditions for stability. We define a function $G(\kappa)$ which is well behaved at infinity

$$
G(\kappa) = \frac{D(\kappa)}{\kappa^2 + \Lambda^2}, \tag{63}
$$

where $D(\kappa)$ is determined by Eq. (32) and Λ^2 is a real, large, positive constant. $G(\kappa)$ has a pole in the upper half of the κ-plane.

In constructing the Nyquist stability diagram, it is useful to list the following properties of I_1 and I_4 (we here consider only distribution functions for which $\partial f_0/\partial J \leq 0$):

a) They are functions only of κ and not of λ.

b) They are complex functions of κ/Ω_0 which are of order unity for smooth distribution functions.

c) At $\kappa = 0$, $I_4(0) = C$ and $I_1(0)$ is given by Eq. (61); they are purely real.

d) At $\kappa = \infty$, they vary as $-1/\kappa^2$; their imaginary parts fall off rapidly to zero.

e) For $\kappa = \kappa_r + i\epsilon(\epsilon \to 0)$, their imaginary parts, arising from bounce resonances ($m\Omega = \kappa_r$), are odd in κ such that $\kappa_r I_i > 0$, where we denote the real and imaginary parts of I by I_r, I_i.

Hence, it follows that

$$G = \left(1 - \lambda^2/\omega^2\right) > 0 \qquad \text{for} \qquad |\kappa| \to \infty.$$

$$G = \frac{1}{\Lambda^2}\left[\lambda^2\left(1 - \frac{V_g}{V}\right)^2 - \tilde{\lambda}^2\left(\tilde{\lambda}^2 + \eta\left(C - I_1\right)\right)\right] \qquad \text{at} \qquad \kappa = 0$$

and for arbitrary $\kappa = \kappa_r + i\varepsilon$, $\epsilon \to 0$,

$$\mathrm{Im}(G) = \frac{1}{(\kappa^2 + \Lambda^2)}\left[\left(\tilde{\lambda}^2 + \eta C - \eta I_{1r}\right) I_{4i} + \left(\tilde{\lambda}^2 + \eta C - \eta I_{4r}\right) I_{1i}\right] \tag{64}$$

and

$$\mathrm{Re}(G) = \frac{1}{(\kappa^2 + \Lambda^2)}\left[\left(\kappa - \lambda\left(1 - \frac{V_g}{V}\right)\right)^2 + \eta^2 I_{1i} I_{4i} - \left(\tilde{\lambda}^2 + \eta C - \eta I_{1r}\right)\left(\tilde{\lambda}^2 + \eta C - \eta I_{4r}\right)\right]. \tag{65}$$

By using Eq. (64) to solve for $\left(\tilde{\lambda}^2 + \eta C - \eta I_{1r}\right)$ and recalling that $I_{1i}/I_{4i} > 0$, we note that for all κ such that $\mathrm{Im}(G) = 0$, $\mathrm{Re}(G) > 0$. (This does not apply for $\kappa = 0$ where I_{1i}

and I_{4i} vanish so that we cannot solve Eq. (64).) We note also that $\mathrm{Im}(G) > 0$ as $|\kappa| \to \infty$, since $\kappa I_{1i} > 0$ and $\kappa I_{4i} > 0$.

We may now plot the Nyquist stability diagram as κ moves along the real axis from $-\infty$ to $+\infty$. We consider the following regimes of parameter space:

1. $\tilde{\lambda}^2(0) + \eta\,(C - I_1(0)) > 0, \qquad G(0) > 0.$

   As $|\kappa| \to \infty$, $G \to 1 - \lambda^2/\omega^2$ in the first quadrant. Near $\kappa = 0$, $\kappa G_i > 0$, and the G-contour crosses the positive real axis from the fourth quadrant to the first quadrant as κ moves through zero from negative to positive values. For κ finite, the contour crosses the real axis only for positive values of G. Thus, the contour must have the form shown in Fig. 5, and it does not encircle the origin. Hence, in addition to one pole, G must have a zero in the upper half of the κ-plane, implying one unstable mode.

2. $\tilde{\lambda}^2(0) + \eta\,(C - I_1(0)) > 0, \qquad G(0) < 0.$

   The G-contour crosses the negative real axis from the third quadrant to the second quadrant as κ moves through zero from negative to positive values. The contour therefore encircles the origin in the negative sense as shown in Fig. 6, and there are no unstable roots.

3. $\tilde{\lambda}^2(0) + \eta\,(C - I_1(0)) < 0.$

   This inequality implies $G(0) > 0$, and the contour cannot encircle the origin, implying one unstable mode.

We therefore conclude that a necessary and sufficient condition for stability is $\tilde{\lambda}^2(0) + \eta\,(C - I_1(0)) > 0$, $G(0) < 0$, that is,

$$\left[\tilde{\lambda}^2(0) + \eta\,(C - I_1(0))\right] - \frac{\omega\,(1 - V_g/V)^2}{1/V - 1} \;>\; 0.$$

The most difficult frequency to stabilize is $\tilde{\lambda} = 0$, so that our general stability condition is

$$\eta\left(C - I_1(0)\right) - \frac{\omega\left(1 - V_g/V\right)^2}{1/V - 1} \;>\; 0. \tag{66}$$

For electrons at the bottom of the well, this inequality reduces to Eq. (37). By using the resonance condition $\omega \approx k_s \approx \frac{k_w}{(1/V-1)}$ we can express Eq. (66) in a more transparent form

$$C - I_1(0) - \frac{k_w}{\eta}\left(\frac{1 - V_g/V}{1/V - 1}\right)^2 \;>\; 0,$$

since k_w/η, the ratio of wiggler wavenumber to the characteristic e-folding distance, is usually very large, stability requires $C > I_1(0)$ and $1 - V_g/V \approx 0$.

1. Linear growth rate (finite "slippage" $(1 - V_g/V) \neq 0$)

In order to obtain estimates of the unstable sideband growth rates, let us assume that the stability criterion (Eq. (66)) is strongly violated

$$\left(1 - \frac{V_g}{V}\right)^2 \gg \frac{\eta}{\omega}\left(C - I_1(0)\right)\left(\frac{1}{V} - 1\right).$$

We look for solutions $\kappa = \lambda\left(1 - V_g/V\right) + \delta$, where $|\lambda\left(1 - V_g/V\right)| \ll |\delta|$. The dispersion relation for δ, obtained from Eq. (32) with $S = 0$, may then be approximated by

$$\delta^2 - \left[\left(\tilde{\lambda}^2 + \eta C - \eta I_1\right)\left(\tilde{\lambda}^2 + \eta C - \eta I_4\right)\right]_{\kappa=\lambda(1-V_g/V)} = 0. \tag{67}$$

For $\lambda^2\left(1 - V_g/V\right)^2 < \Omega_0^2$, we may approximate I_{1r} and I_{4r} by Eqs. (61) and (62), and if $\eta\left(1 - V_g/V\right)^2/\Omega_0^2 > \left(1 - V_g\right)/\omega V$, we obtain the unstable sideband gain

$$\delta = \frac{i\lambda\left(1 - V_g/V\right)}{\Omega_0}\left[\eta^2\left(C - I_1(0)\right)\right]^{1/2}. \tag{68}$$

We have neglected contributions from I_{1i}, I_{4i}.

If $\left[\left(\tilde{\lambda}^2 + \eta C - \eta I_{1r}\right)\left(\tilde{\lambda}^2 + \eta C - \eta I_{4r}\right) + I_{1i}I_{4i}\right]_{\kappa=\lambda(1-V_g/V)} > 0$, we would have to keep the contributions from I_{1i} and I_{4i} to evaluate the unstable sideband gain.

2. Linear growth rate (zero "slippage" $(1 - V_g/V) = 0$)

We now consider the limit $(1 - V_g/V) = 0$ where slippage between the electrons and signal is eliminated by using a waveguide. For κ small, the dispersion relation may be approximated by

$$\kappa^2 - \tilde{\lambda}^2(0)\left[\tilde{\lambda}^2(0) + \eta C - \eta I_1(0)\right] - \left[\kappa\frac{\partial}{\partial\kappa} + \frac{\kappa^2}{2}\frac{\partial^2}{\partial\kappa^2} + \cdots\right]\left[\left(\tilde{\lambda}^2 + \eta C - \eta I_1\right)\left(\tilde{\lambda}^2 + \eta C - \eta I_4\right)\right]_{\kappa=0} = 0. \quad (69)$$

Ignoring terms of order λ/ω, we see from our previous discussion that the first derivative term must be imaginary and of order η^2/Ω_0^2, while the second term must be real and of order η^2/Ω_0^2. Hence, the inclusion of these terms would change κ by order $\eta^2/\Omega_0^2 \ll 1$. We may therefore neglect them and solve immediately for κ. If $\eta\left(C - I_1(0)\right) < 0$ so that we violate our stability criterion, and if we choose the worst $\tilde{\lambda}^2(0)$ values, $\tilde{\lambda}^2(0) = \frac{\eta}{2}\left(I_1(0) - C\right)$, we obtain the unstable root

$$\kappa = \frac{i\eta}{2}\left(I_1(0) - C\right). \quad (70)$$

From Eqs. (58) and (61) we note that

$$C - I_1(0) = -\int dJ \frac{\partial f_0}{\partial J}\Omega_0 P_0\left(k^2(J)\right) = \int dJ\, f_0 P_0'\left(k^2(J)\right) \quad (71)$$

$$P_0\left(k^2\right) = \frac{8}{\pi}\left\{E\left(\frac{E}{K} - 1\right) + \frac{2}{3}\left(2k^2E - E + k'^2K\right)\right\} \quad (72)$$

$$P_0' = \Omega_0\frac{\partial P_0}{\partial J} = \frac{1}{k^2}\left(\frac{E}{K} - 1\right)\left(\frac{2E}{K} - 1\right) + 2\left(\frac{2E}{K} - 1\right) - \frac{1}{k^2k'^2}\frac{E^2}{K^2}\left(\frac{E}{K} - k'^2\right). \quad (73)$$

It may be verified that for electrons all at the bottom of the well $f_0 = \delta(J)$,

$$C - I_1(0) = 1$$

and for electrons filling the well all the way to the top $f_0 = 1/J_{\max}$, $J < J_{\max}$,

$$C - I_1(0) = -\frac{1}{3}.$$

In Fig. 7, we plot P_0 and P_0' as a function of $\hat{J} = J/J_{\max}$, $J_{\max} = 8\Omega_0/\pi$. It may be seen that electrons with $\hat{J} < .51$ are stabilizing, those with $\hat{J} > .51$ are destabilizing. Hence while uniformly filled wells are unstable, a distribution with most of the electrons having $\hat{J}$ below .51 would be stable for this case of $(1 - V_g/V) = 0$.

3. Special cases

We will now calculate the sideband growth rates for two specific trapped distribution functions: i) $f_0 = \frac{1}{J_{\max}}$, $J < J_{\max} \cong \frac{8\Omega_0}{\pi}$; ii) $f_0 = \frac{9\pi}{32\Omega_0}(1 - k^2(J))$, $1 > k^2 > 0$. For purposes of comparison with numerical simulations, we further restrict the discussion to the regime where

$$(1 - V_g/V)^2 > \frac{\Omega_0^2 (1 - V_g)}{\omega\eta}$$

and we look for solutions

$$\kappa \sim \lambda\left(1 - \frac{V_g}{V}\right) \sim \lambda\left(\frac{1}{V} - 1\right) \lesssim \Omega_0.$$

We may then approximate the dispersion relation by

$$D(\kappa) = \left[\kappa - \lambda\left(1 - \frac{V_g}{V}\right)\right]^2 - \eta^2 (C - I_1)(C - I_4) = 0. \tag{74}$$

a. Full bucket distribution function f_0

If the electrons fill the ponderomotive well all the way to the top, a distribution that might result from very adiabatic trapping, the distribution function f_0 may be represented by

$$f_0 = \frac{1}{J_{\max}}, \qquad J < J_{\max} = \frac{8\Omega_0}{\pi}.$$

Substituting for f_0 in the integrals, we obtain

$$\begin{aligned} C &= \int_0^{J_{\max}} dJ \left(\frac{2E}{K} - 1\right) = \frac{1}{3} \\ I_1 &= -\sum_{m \text{ even}} \frac{\pi^5 m^3 q^m \Omega_0}{8K^4 (1 - q^m)^2 (\kappa - m\Omega)} \Bigg|_{k^2 \to 1} \end{aligned}$$

$$I_4 = -\sum_{m \text{ odd}} \frac{\pi^5 m^3 q^m \Omega_0}{8K^4 (1+q^m)^2 (\kappa - m\Omega)} \Big|_{k^2 \to 1}.$$

Since $K \to \infty$ as $k^2 \to 1$, we may convert the m-summation in I_1 into an integral in $\theta = m\pi^2/4K$ $(d\theta = \pi^2/4K)$

$$I_1 = -\frac{2}{\pi^2} \int_{-\infty}^{+\infty} d\theta \frac{\theta^3}{\sinh^2 \theta(\rho - \theta)},$$

where $\rho = \pi\kappa/2\Omega_0$. By deforming the integration contour in the θ-plane to enclose the poles at $\sinh\theta = 0$, we may write I_1 as an infinite sum

$$I_1 = -i\left\{\frac{2\pi^2 y^3}{\sinh^2 \pi y} + i\left[\frac{2}{3} - 4y^2 + 8y^4 \sum_{N=0}^{\infty} \frac{N+1}{((N+1)^2+y^2)^2}\right]\right\}, \tag{75}$$

where $y = \rho/\pi = \kappa/2\Omega_0$.

Similarly, for I_4:

$$\begin{aligned} I_4 &= -\frac{2}{\pi^2} \int_{-\infty}^{+\infty} d\theta \frac{\theta^3}{\cosh^2 \theta(\rho - \theta)} \\ &= -i\left\{\frac{2\pi^2 y^3}{\cosh^2 \pi y} + i\left[\frac{1}{3} + 4y^2 - 8y^4 \sum_{N=0}^{\infty} \frac{(N+1/2)}{((N+1/2)^2+y^2)^2}\right]\right\}. \end{aligned} \tag{76}$$

The dispersion relation is

$$\left[\kappa - \lambda\left(1 - \frac{V_g}{V}\right)\right]^2 - \eta^2\left(\frac{1}{3} - I_1\right)\left(\frac{1}{3} - I_4\right) = 0. \tag{77}$$

Let $\kappa = \lambda(1 - V_g/V) + \delta$, with $|\delta| < |\lambda(1 - V_g/V)|$. The unstable root is determined by

$$\delta^2 = \eta^2\left(\frac{1}{3} - I_1\right)\left(\frac{1}{3} - I_4\right)\Big|_{\kappa = \lambda(1 - V_g/V)}. \tag{78}$$

The imaginary part of δ/η is tabulated for various values of κ/Ω_0 in Table I, and it is plotted as a function of κ/Ω_0 in Fig. 8. For comparison, we also plot in Fig. 8 the corresponding gain curve for the "old" theory[1] and it will be noted that the predicted sideband gains are essentially the same.

For $\kappa/\Omega_0 = \lambda(1 - V_g/V)/\Omega_0 \ll 1$, $I_1 \to 2/3 - i\kappa/\Omega_0$, $I_4 \to 1/3 + \kappa^2/\Omega_0^2$, and

$$\delta^2 = \frac{\eta^2}{3}\frac{\kappa^2}{\Omega_0^2}\left(1 - \frac{i3\kappa}{\Omega_0}\right).$$

The sideband gain is a maximum at $\kappa/\Omega_0 \sim 1$.

b. Monotonic decreasing distribution function f_0

If $f_0(J)$ decreases linearly in $k^2(J)$ from the bottom to the top of the ponderomotive well, a more or less "typical" trapped distribution, f_0 may be represented by

$$f_0 = \frac{9\pi}{32\Omega_0}\left(1-k^2\right), \qquad 1 > k^2 > 0.$$

The integrals in J may be transformed to integrals in k^2,

$$\int dJ \to \int dk^2 \frac{4\Omega_0}{\pi} K.$$

Thus

$$C = \int dJ\, f_0 \left(\frac{2E}{K} - 1\right) = 0.6$$

and the integrals I_1 and I_4 may be determined numerically from Eqs. (41) and (42).

The dispersion relation is

$$D(\kappa) = \left[\kappa - \lambda\left(1 - \frac{V_g}{V}\right)\right]^2 - \eta^2\,(0.6 - I_1)\,(0.6 - I_4) = 0. \tag{79}$$

With $\kappa = \lambda\,(1 - V_g/V) + \delta$, $|\delta| < |\lambda\,(1 - V_g/V)|$, the unstable root is determined by

$$\delta^2 = \eta^2\,(0.6 - I_1)\,(0.6 - I_4)\,\Big|_{\kappa=\lambda(1-V_g/V)}. \tag{80}$$

For $\kappa^2/\Omega^2 \ll 1$,

$$I_4 \to 0.6 + \frac{\kappa^2}{\Omega_0^2} +, \qquad \cdot I_1 \to 0.22$$

the unstable root is

$$\delta = i0.62\eta \left|\lambda\left(1 - \frac{V_g}{V}\right)\right|.$$

In Fig. 9, we plot $\mathrm{Im}(\delta/\eta)$ as a function of κ/Ω_0. I_1 and I_4 were evaluated by numerical integration using Eqs. (59) and (60). Ten terms in each sum were sufficient to obtain convergence.

The linear sideband gain increases linearly with κ/Ω_0 for $\kappa/\Omega_0 < 1$ and reaches a maximum $\mathrm{Im}(\delta/\eta) = .52$ for $\kappa/\Omega_0 \approx .75$.

In Sec. V, we discuss the simulation of the linear gain of sideband modes using a particle pushing simulation code for this distribution. The results of these simulations are also plotted in Fig. 9. The agreement between theory and simulations is satisfactory.

B. Tapered wiggler

In the case of a tapered wiggler where $\sin\psi_r \neq 0$, the electron equilibrium orbits and hence the coefficients α_m, β_m are not expressible in terms of simple functions, except in the extreme limit of all electrons trapped at the bottom of the well.

For smooth distribution functions, the integrals I_1, I_2, I_3, I_4 have no singularities. However, they are complex functions of κ/Ω_0, their imaginary parts originating from the bounce resonant interactions of the trapped electrons with the sideband modes. Thus, a general Nyquist stability analysis for a tapered wiggler will differ from that described in Sec. IIIB, and requires an extension of the discussion in Sec. IVA to include finite $S \neq 0$.

The imaginary part of G (defined by Eq. (63)) for $\kappa = \kappa_r + i\epsilon$, $\epsilon \to 0$ is

$$\begin{aligned} \mathrm{Im}(G) &= \frac{1}{(\kappa^2+\Lambda^2)}\Big[2\left(\kappa - \lambda\left(1-\frac{V_g}{V}\right)\right)\eta S + 2\eta^2 I_{2r} I_{2i} \\ &\quad + \eta\left(\tilde{\lambda}^2 + \eta C - \eta I_{4r}\right) I_{1i} + \eta\left(\tilde{\lambda}^2 + \eta C - \eta I_{1r}\right) I_{4i}\Big]. \end{aligned} \tag{81}$$

The I-integrals are at most of $O(1)$ (for smooth distribution functions) and I_{1i}, I_{2i}, $I_{3i} \sim O\left(\kappa/\Omega_0\right)$ for $\kappa/\Omega_0 < 1$.

If we assume that $S \sim O(1)$, $\lambda\left(1 - V_g/V\right) > \eta$, $\lambda^2/\omega(1/V - 1) \sim \eta \ll \Omega_0$, we may approximate $\mathrm{Im}(G)$ by the first term

$$\mathrm{Im}(G) \approx \frac{2\eta S\left(\kappa - \lambda\left(1 - V_g/V\right)\right)}{\left(\kappa^2+\Lambda^2\right)}. \tag{82}$$

In this regime of parameter space, $\mathrm{Im}(G) = 0$ at $\kappa = \lambda\left(1 - V_g/V\right)$, and it may be verified that a Nyquist plot of $G(\kappa)$ yields a contour which encircles the origin (implying stability)

whenever $\mathrm{Re}(G) < 0$ at $\kappa = \lambda(1 - V_g/V)$, or equivalently

$$\begin{aligned}
\hat{D}_r &\equiv D_r(\kappa)\Big|_{\kappa=\lambda(1-V_g/V)} \\
&\equiv -\left[\eta^2\left(S^2 - I_{2r}^2 + I_{2i}^2\right) + \left(\tilde{\lambda}^2 + \eta C - \eta I_{1r}\right)\left(\tilde{\lambda}^2 + \eta C - \eta I_{4r}\right) - \eta^2 I_{4i} I_{1i}\right]_{\kappa=\lambda(1-V_g/V)} \\
&< 0. \qquad (83)
\end{aligned}$$

An unstable root exists if $\hat{D}_r > 0$. To obtain an estimate of the unstable sideband growth rates, we look for solutions $\kappa = \lambda(1 - V_g/V) + \delta$, where $\Omega_0 > |\lambda(1 - V_g/V)| > |\delta|$. The dispersion relation may then be approximated by

$$(\delta + i\eta S)^2 = -\eta^2 S^2 - \hat{D}_r - i\hat{D}_i, \qquad (84)$$

where

$$\begin{aligned}
\hat{D}_i &\equiv D_i(\kappa)\Big|_{\kappa=\lambda(1-V_g/V)} \\
&= \left[2\eta^2 I_{2r} I_{2i} + \eta\left(\tilde{\lambda}^2 + \eta C - \eta I_{1r}\right) I_{4i} + \eta\left(\tilde{\lambda}^2 + \eta C - \eta I_{4r}\right) I_{1i}\right]_{\kappa=\lambda(1-V_g/V)}.
\end{aligned}$$

As mentioned earlier this case only appears tractable if we further assume $\frac{\lambda(1-V_g/V)}{\Omega_0} = \kappa/\Omega_0 < 1$, so we can simplify the integrals I_{1r}, $I_{2r} = I_{3r}$, I_{4r} by expanding in a power series in κ/Ω_0. We assume no resonant particles with $\Omega = 0$ so that I_{1i}, I_{2i}, I_{4i} may be neglected in this limit, i.e., $\hat{D}_i = 0$. Then stability depends only on $\hat{D}_r$.

Thus

$$I_1(0) = -\int dJ \frac{\partial f_0}{\partial J}\frac{\Omega_0^2}{\Omega}\sum_{m\neq 0}\oint\frac{d\phi}{2\pi}\cos\psi e^{im\phi}\oint\frac{d\phi'}{2\pi}\cos\psi e^{-im\phi}.$$

Using the fact that

$$\sum_{m=-\infty}^{m=+\infty} e^{im(\phi-\phi')} = 2\pi\delta(\phi - \phi')$$

we may rewrite

$$\begin{aligned}
I_1(0) &= -\Omega_0^2\int\frac{dJ}{\Omega}\frac{\partial f_0}{\partial J}\left[\overline{\overline{\cos^2\psi}} - \overline{\overline{\cos\psi}}^2\right] \\
&= -\Omega_0^2\int\frac{dJ}{\Omega}\frac{\partial f_0}{\partial J}\overline{\overline{\left[\cos\psi - \overline{\overline{\cos\psi}}\right]^2}}, \qquad (85)
\end{aligned}$$

where the double bar signifies an average over ϕ for a given J

$$\overline{\overline{\cos\psi}} = \oint \frac{d\phi}{2\pi} \cos\psi.$$

For convenience, we have set $\xi_0 = 0$.

Similarly

$$\begin{aligned} I_{4r} &= -\int dJ \frac{\partial f_0}{\partial J} \frac{\Omega_0^2}{\Omega} \sum_{m\neq 0} \left(1 + \frac{\kappa^2}{m^2\Omega^2} + \cdots\right) \oint \frac{d\phi}{2\pi} \sin\psi e^{im\phi} \oint \frac{d\phi'}{2\pi} \sin\psi e^{-im\phi'} \\ &= -\Omega_0^2 \int \frac{dJ}{\Omega} \frac{\partial f_0}{\partial J} \left[\overline{\overline{\sin^2\psi}} - \overline{\overline{\sin\psi}}^2\right] - \Omega_0^2 \int \frac{dJ}{\Omega} \frac{\partial f_0}{\partial J} \sum_{m\neq 0} \frac{\kappa^2}{m^2\Omega^2} \overline{\overline{\sin\psi e^{im\phi}}}\, \overline{\overline{\sin\psi e^{-im\phi}}}. \end{aligned}$$

This may be simplified further by using

$$\frac{d\phi}{d\psi} = \frac{\Omega dz}{d\psi} = \frac{\Omega}{p(\psi, H_0)},$$

where

$$p(\psi, H_0) = \text{sign}\left(\frac{d\psi}{dz}\right) \left\{2H_0 + 2\Omega_0^2 (\cos\psi + \psi \sin\psi_r)\right\}^{1/2}.$$

Hence

$$\begin{aligned} \overline{\overline{\sin\psi}} &= \Omega \int \frac{d\psi}{2\pi} \frac{(\sin\psi - \sin\psi_r + \sin\psi_r)}{p(\psi, H_0)} \\ &= \sin\psi_r \\ \overline{\overline{\sin^2\psi}} &= \Omega \int \frac{d\psi}{2\pi} \frac{[\sin\psi - \sin\psi_r + \sin\psi_r]^2}{p(\psi, H_0)} \\ &= \sin^2\psi_r + \frac{\Omega}{2\pi} \int d\psi \frac{(\sin\psi - \sin\psi_r)^2}{p(\psi, H_0)} \\ &= \sin^2\psi_r + \frac{\Omega}{\Omega_0^2} \int \frac{d\psi}{2\pi} \cos\psi p(\psi, H_0) \\ \overline{\overline{\sin\psi e^{im\phi}}} &= \Omega \int \frac{d\psi}{2\pi} \frac{(\sin\psi - \sin\psi_r + \sin\psi_r) e^{im\phi}}{p(\psi, H_0)} \\ &= -im \frac{\Omega^2}{\Omega_0^2} \int \frac{d\psi}{2\pi} e^{im\phi}. \end{aligned}$$

Therefore,

$$\begin{aligned} I_{4r} &= -\int dJ \frac{\partial f_0}{\partial J} \int \frac{d\psi}{2\pi} \cos\psi p\left(\psi, H_0\right) - \frac{\kappa^2}{\Omega_0^2} \int dJ \frac{\partial f_0}{\partial J} \int \frac{d\psi}{2\pi} p^2\left(\psi, H_0\right) \\ &= \int dJ\, f_0 \oint \frac{d\phi}{2\pi} \cos\psi + \frac{\kappa^2}{\Omega_0^2} \int dJ\, f_0 \\ &= C + \frac{\kappa^2}{\Omega_0^2} \end{aligned} \tag{86}$$

and

$$S = \int dJ\, f_0 \oint \frac{d\phi}{2\pi} \sin\psi = \sin\psi_r. \tag{87}$$

Furthermore,

$$\begin{aligned} I_{2r} &= I_{3r} \\ &= -\int dJ \frac{\partial f_0}{\partial J} \frac{\Omega_0^2}{\Omega} \sum_{m\neq 0} \left(1 + \frac{\kappa^2}{m^2\Omega^2} + \cdots\right) \oint \frac{d\phi}{2\pi} \sin\psi e^{-im\phi} \oint \frac{d\phi'}{2\pi} \cos\psi e^{im\phi'} \\ &= -S + \frac{\kappa^2}{\Omega_0^2} I''_{2r}(0), \end{aligned} \tag{88}$$

where

$$I''_{2r}(0) = -\Omega_0^2 \int \frac{dJ}{\Omega} \frac{\partial f_0}{\partial J} \left[\overline{\overline{\psi\cos\psi}} - \overline{\overline{\psi}}\,\overline{\overline{\cos\psi}}\right]. \tag{89}$$

Substituting these expressions for the I-integrals in Eq. (83) for $D_r(\kappa)$, and neglecting the contributions due to I_{1i}, I_{2i}, I_{4i} (we assume the number of resonant electrons to be small for $\kappa/\Omega_0 \ll 1$), we obtain

$$D_r(\kappa) \approx \frac{\eta^2\kappa^2}{\Omega_0^2}\left(C - I_1(0) - 2SI''_{2r}(0)\right) - \tilde{\lambda}^4 - \tilde{\lambda}^2\eta\left(C - I_1(0)\right).$$

The sideband modes are unstable if $\hat{D}_r > 0$. This can be satisfied when

$$\left(1 - \frac{V_g}{V}\right)^2 \left[C - I_{1r}(0) - 2SI''_{2r}(0)\right] - \frac{\Omega_0^2}{\eta\omega V}\left(1 - V_g\right)\left(C - I_1(0)\right) > 0. \tag{90}$$

1. Normal slippage

For the usual, not very low current, case:

$$\left(1-\frac{V_g}{V}\right)^2 \gg \frac{\Omega_0^2}{\eta\omega V}\left(1-V_g\right),$$

$$(\delta+i\eta S)^2 = -\eta^2 S^2 - \frac{\eta^2\lambda^2\left(1-V_g/V\right)^2}{\Omega_0^2}\left[C - I_{1r}(0) - 2SI''_{2r}(0)\right], \tag{91}$$

where

$$C - I_{1r}(0) - 2SI''_{2r}(0) = -\int dJ\frac{\partial f_0}{\partial J}\Omega_0 Q(J,S) \tag{92}$$

and

$$Q(J,S) \equiv \frac{\Omega_0}{\Omega}\left\{\overline{\overline{\sin^2\psi}} - \overline{\overline{\sin\psi}}^2 - \overline{\overline{\cos^2\psi}} + \overline{\overline{\cos\psi}}^2 - 2S\overline{\overline{\psi\cos\psi}} - \overline{\overline{\psi}}\,\overline{\overline{\cos\psi}}\right\} \tag{93}$$

$$\begin{aligned}
\frac{\Omega_0}{\Omega}\left\{\overline{\overline{\sin^2\psi}} - \overline{\overline{\sin\psi}}^2\right\} &= \frac{1}{\pi\Omega_0}\int_{\psi_{\min}}^{\psi_{\max}} d\psi\cos\psi p\left(\psi,H_0\right) \\
\frac{\Omega_0}{\omega}\left\{\overline{\overline{\cos^2\psi}} - \overline{\overline{\cos\psi}}^2 + 2S\left[\overline{\overline{\psi\cos\psi}} - \overline{\overline{\psi}}\,\overline{\overline{\cos\psi}}\right]\right\} &= \frac{\Omega_0}{\Omega}\left\{\left(\overline{\overline{\cos\psi+s\psi}}\right)^2 - \left(\overline{\overline{\cos\psi+s\psi}}\right)^2\right. \\
&\quad \left. - S^2\left[\left(\overline{\overline{\psi-\pi+\psi_r}}\right)^2 - \left(\overline{\overline{\psi-\pi+\psi_r}}\right)^2\right]\right\} \\
&= \frac{1}{4\Omega_0^3}\int_{\psi_{\min}}^{\psi_{\max}}\frac{d\psi}{\pi}p^3\left(\psi,H_0\right) - \frac{\Omega}{4\Omega_0^3}\left(\int_{\psi_{\min}}^{\psi_{\max}}\frac{d\psi}{\pi}p\left(\psi,H_0\right)\right)^2 \\
&\quad - S^2\Omega_0\int_{\psi_{\min}}^{\psi_{\max}}\frac{d\psi}{\pi}\frac{\left(\psi-\psi_{\max}\right)^2}{p\left(\psi,H_0\right)} + S^2\Omega_0\Omega\left(\int_{\psi_{\min}}^{\psi_{\max}}\frac{d\psi}{\pi}\frac{\left(\psi-\psi_{\max}\right)}{p\left(\psi,H_0\right)}\right)^2.
\end{aligned}$$

As $J\to 0$,

$$Q(J,S) \;\to\; \frac{J}{\Omega_0\cos\psi_r}$$

and in the limit $f_0(J)=\delta(J)$,

$$C - I_{1r}(0) - 2SI''_{2r}(0) \;\to\; \frac{1}{\cos\psi_r} > 0,$$

and we recover the dispersion relation (Eq. (46)) previously derived in Sec. IIIB.

We have calculated numerically the orbit averages required to evaluate $Q(J,S)$ for values of $S = 0.05,\ 0.2,\ 0.5,\ 0.8$. In Fig. 10, we plot $Q(J,S)$ as a function of $\hat{J} = J/J_{\max}$, where

$J_{\max} = 8\Omega_0/\pi$ is the magnitude of J at the separatrix for $S = 0$. As the tapering parameter S increases, the magnitude of J at the separatrix decreases, and the graphs of Q terminate at values of $\hat{J}$ less than unity.

When $S \gtrsim 0.5$, $\partial Q/\partial J > 0$ and therefore all the trapped electrons are destabilizing.

For values of $S > 0.12$, Q is positive, and the condition for instability is satisfied for electron distribution functions $\partial f_0/\partial J < 0$.

Thus there remains the possibility that for $S < .12$, the sidebands might be stable. From Fig. 10, we can see that this could only happen for a distribution function where $\partial f_0/\partial J = 0$ except for values of J very close to the separatrix. However, from Fig. 8 ($S = 0$), we conclude that such distribution functions are in fact almost certainly unstable for $\kappa/\Omega_0 \sim O(1)$.

In determining the critical value of S above which $Q > 0$, it is necessary to calculate Q accurately for particles near the separatrix where Q varies rapidly. As a check on our numerical results, we make an analytic evaluation of Q for particles at the separatrix in the limit of small $S = \sin\psi_r \ll 1$.

For $S = 0$, $Q\left(J, S = 0\right) = P_0\left(k^2(J)\right)$, where P_0 is defined by Eq. (72), and it may readily be verified that $Q \to -8/3\pi$ at the separatrix where $\Omega \to 0$, $k^2(J) \to 1$, $\hat{J} \to 1$.

For finite but small S, we note that

$$\frac{\Omega_0}{\Omega}\left\{\overline{\overline{\cos^2\psi}} - \overline{\overline{\cos\psi}}^2 + 2S\left[\overline{\overline{\psi\cos\psi}} - \overline{\overline{\psi}}\,\overline{\overline{\cos\psi}}\right]\right\} \approx \frac{1}{4\Omega_0^3}\int_{\psi_{\min}}^{\psi_{\max}} \frac{d\psi}{\pi} p^3\left(\psi, H_0\right) + O\left(S^2\right)$$

$$\approx \frac{16}{3\pi} - 6S + \text{higher order terms in } S$$

and

$$\frac{\Omega_0}{\Omega}\left(\overline{\overline{\sin^2\psi}} - \overline{\overline{\sin\psi}}^2\right) = \frac{1}{\Omega_0}\int_{\psi_{\min}}^{\psi_{\max}} \frac{d\psi}{\pi}\cos\psi p\left(\psi, H_0\right)$$

$$\approx \frac{8}{3\pi} - 3S + S\ln\frac{16}{\pi s} + \text{higher order terms in } S.$$

Thus, we obtain for $Q(J, S)$ in the limit of $S \ll 1$ and $H_0/\Omega_0^2 \to 1 - \pi S$

$$Q(J, S) \to -\frac{8}{3\pi} + 3S + S\ln\frac{16}{\pi S}.$$

This expression for Q predicts a critical value of $S = .126\,(Q = 0)$, which is close to that evaluated numerically.

2. Low slippage

For

$$\left(1 - \frac{V_g}{V}\right)^2 \ll \frac{\Omega_0^2}{\eta\omega V}(1 - V_g)\,,$$

$$(\delta + i\eta S)^2 = -\eta^2 S^2 + \frac{\lambda^2}{\omega V}(1 - V_g)\left[\eta\,(C - I_{1r}(0)) + \frac{\lambda^2}{\omega V}(1 - V_g)\right], \tag{94}$$

where

$$C - I_{1r}(0) \;=\; -\int dJ \frac{\partial f_0}{\partial J}\Omega_0 P\,(J, \sin\psi_r) \tag{95}$$

$$P\,(J, \sin\psi_r) \;=\; \frac{\Omega_0}{\Omega}\left\{\overline{\overline{\sin^2\psi}} - \overline{\overline{\sin\psi}}^2 - \overline{\overline{\cos^2\psi}} + \overline{\overline{\cos\psi}}^2\right\} \tag{96}$$

and $P > 0$ implies stability ($\partial f_0/\partial J < 0$).

As $J \to 0$

$$P\,(J, \sin\psi_r) \;\to\; \frac{J}{\Omega_0}\left(\cos\psi_r - \frac{\sin^2\psi_r}{\cos\psi_r}\right).$$

In the limit $f_0(J) = \delta(J)$,

$$C - I_{1r}(0) \;\to\; \cos\psi_r - \frac{\sin^2\psi_r}{\cos\psi_r}$$

and we recover the dispersion relation (Eq. (46)) previously derived in Sec. IIIB.

In Fig. 11, we plot $P\,(J, \sin\psi_r)$ as a function of $\hat{J} = J/J_{\max}$ for various values of $\sin\psi_r$. When $\psi_r > \pi/4$, $\partial P/\partial J < 0$, and therefore all the trapped electrons are destabilizing. For $\psi_r < \pi/4$, it is difficult to make a definite statement, although the results of Sec. III leads us to think stability is unlikely.

V. Numerical Simulations

The linear growth of sideband modes in untapered and tapered wigglers has been simulated for free electron lasers in which the slippage between beam electrons and optical pulse is

nonzero. A 1-D time dependent particle pushing code (described in detail in Ref. 14) was used in these simulations.

The optical pulse was considered to be an electromagnetic signal propagating in free space with group velocity equal to the velocity of light. The electrons and the "photons" of the electromagnetic signal were followed along their respective characteristics, namely the longitudinal beam velocity V and the signal group velocity $V_g = 1$. Thus, transforming from z and t to new independent variables u and v defined by

$$u = \frac{1}{(1/V-1)}\left(\frac{z}{V}-t\right)$$

$$v = \frac{1}{(1/V-1)}(t-z)$$

we obtain from Eq. (5) and Eq. (13)

$$\frac{\partial \psi}{\partial v} = p \tag{97a}$$

$$\frac{\partial p}{\partial v} = \Omega_0^2 \sin\psi_r - \frac{\Omega_0^2}{a_0}\left(\alpha_0 \sin\psi + \alpha_s \cos\psi\right) \tag{97b}$$

$$\frac{\partial \alpha_c}{\partial u} = \frac{4\pi n_0 e^2 a_w}{m\gamma}\int \frac{d\psi_0 dp_0}{2\pi}\bar{f}_0\left(\psi, p_0\right)\sin\psi \tag{98a}$$

$$\frac{\partial \alpha_s}{\partial u} = \frac{4\pi n_0 e^2 a_w}{m\gamma}\int \frac{d\psi_0 dp_0}{2\pi}\bar{f}_0\left(\psi_0, p_0\right)\cos\psi, \tag{98b}$$

where

$$\alpha_c \equiv a\cos\xi$$

$$\alpha_s \equiv a\sin\xi$$

and we have neglected terms in Eq. (13) proportional to second derivatives in space and time.

In the u–v plane shown in Fig. (12), the electron beam is divided into beamlets which move horizontally along lines of u = constant, and the photons of the optical pulse move

vertically along lines of v = constant. The electron beamlets and photons interact when their trajectories cross within the area bounded by the lines $z = u + v = 0$ and $z = u + v = L$, that is, inside the wiggler. L is the wiggler length.

A leap-frog scheme was used to integrate the electron phase space variables (ψ and p) and the photon variables (signal amplitude "a" and phase ξ) from the front to the back of the wiggler.

The simulation was carried out for an electron distribution function $\bar{f}_0$ at the beginning of the wiggler which was linear in the Hamiltonian H_0

$$\bar{f}_0 \propto \frac{(H_{\max} - H_0)}{(H_{\max} - H_{\min})},$$

where $H_0 = p_0^2/2 - \Omega_0^2(\cos(\psi_0 + \xi_0) + \psi_0 \sin\psi_r)$. The electrons were randomly distributed within the trapped region of phase space weighted by a linear function of H_0 as prescribed above. This initial particle load simulates the electron distribution function $f_0(J) \propto 1 - k^2(J)$, $1 > k^2 > 0$, which was one of the examples used in Sec. IVA to calculate the sideband growth rates for an untapered wiggler. It was not possible to simulate the case of a uniformly filled ponderomotive well because of nonlinear detrapping effects on the electrons at the separatrix. The wiggler length was chosen to correspond to four synchrotron periods of an electron at the bottom of the ponderomotive well.

We produce a "quiet start" by choosing the initial distribution for each electron beamlet to be identical at the beginning of the wiggler. Then, if the amplitude and phase of the incident optical signal is time independent (that is, independent of v), it remains time independent as it propagates through the wiggler. This follows because the initial conditions for electrons and photons are identical at $u + v = 0$ and hence the evolution of each electron beamlet and photon is identical to every other beamlet and photon through the wiggler. Thus, their variables will be functions only of the single variable $z = u + v$. Under these conditions, growth of the optical signal without generation of any sidebands can be readily simulated.

In order to induce growth of sideband instabilities, we superimpose a low amplitude time

dependent perturbation on the incident optical signal

$$\alpha_c = \alpha_c^0 + \alpha_c^\wedge \cos \wedge v$$

$$\alpha_s = \alpha_s^0 + \alpha_s^\wedge \sin \wedge v,$$

where

$$\alpha_c^0 = a_0 \cos \xi_0$$

$$\alpha_s^0 = a_0 \sin \xi_0.$$

It should be noted that below the line $u+v=0$ and above the line $u+v=L$, α_c and α_s are independent of the coordinate u. The initial perturbations, $\alpha_c^\wedge(0)$ and $\alpha_s^\wedge(0)$, correspond to sideband frequencies displaced from the main signal by $\lambda = \Lambda/(1/V-1)$.

The linear gain of sideband instabilities is calculated by carrying out two successive simulations: 1) the first with $\alpha_c^\wedge(0) \neq 0$, $\alpha_s^\wedge(0) = 0$; 2) the second with $\alpha_c^\wedge(0)$, $\alpha_s^\wedge(0) \neq 0$. In each simulation, the output optical signal is Fourier transformed in v along a line $u =$ constant above the boundary $u+v=L$, and the variables $\alpha_c^0(L)$, $\alpha_s^0(L)$, $\alpha_c^\wedge(L)$, $\alpha_s^\wedge(L)$ at the end of the wiggler determined. From the ratio of final to initial amplitudes, we can construct the matrix equation

$$\begin{pmatrix} \alpha_c^\wedge(L) \\ \alpha_s^\wedge(L) \end{pmatrix} = \begin{pmatrix} A_{11} & A_{12} \\ A_{21} & A_{22} \end{pmatrix} \begin{pmatrix} \alpha_c^\wedge(0) \\ \alpha_s^\wedge(0) \end{pmatrix}, \tag{99}$$

where the matrix elements A_{ij} are complex quantities.

To ensure linearity, we repeat these simulations with smaller values of $\alpha_c^\wedge(0)$ and $\alpha_s^\wedge(0)$ until the matrix elements A_{ij} are unchanged.

The perturbed signal amplitude $\tilde{a}$ and phase $\tilde{\xi}$ introduced earlier in Sec. II (see Eq. (16)) are related to perturbed α_c and α_s by

$$\begin{pmatrix} \tilde{a}^\wedge \\ \tilde{\xi}^\wedge \end{pmatrix} = \begin{pmatrix} \alpha_c^0 & \alpha_s^0 \\ -\alpha_s^0 & \alpha_c^0 \end{pmatrix} \begin{pmatrix} \alpha_c^\wedge \\ \alpha_s^\wedge \end{pmatrix}.$$

Thus, Eq. (99) may be rewritten as follows:

$$\begin{pmatrix} \tilde{a}\hat{}(L) \\ \tilde{\xi}\hat{}(L) \end{pmatrix} = \begin{pmatrix} B_{11} & B_{12} \\ B_{21} & B_{22} \end{pmatrix} \begin{pmatrix} \tilde{a}\hat{}(0) \\ \tilde{\xi}\hat{}(0) \end{pmatrix}$$

where

$$\begin{pmatrix} B_{11} & B_{12} \\ B_{21} & B_{22} \end{pmatrix} = \begin{pmatrix} \alpha_c^0(L) & \alpha_s^0(L) \\ -\alpha_s^0(L) & \alpha_c^0(L) \end{pmatrix} \begin{pmatrix} A_{11} & A_{12} \\ A_{21} & A_{22} \end{pmatrix} \begin{pmatrix} \alpha_c^0(0) & -\alpha_s^0(0) \\ \alpha_s^0(0) & \alpha_c^0(0) \end{pmatrix}.$$

The eigenvalues $(1+\Delta)$ of the B-matrix are solutions of the equation

$$(B_{11}-1-\Delta)(B_{22}-1-\Delta)-B_{12}B_{21}=0.$$

The linear sideband gain is therefore given by

$$\mathrm{Re}\ln\frac{\tilde{a}\hat{}(L)}{\tilde{a}\hat{}(0)} = \mathrm{Re}\ln(1+\Delta) \approx \mathrm{Re}\,\Delta. \tag{100}$$

In Fig. 9, we plot the results of a number of simulations for $\sin\psi_r = 0.0$. The agreement between the theory and simulations is satisfactory.

Simulations were also done for tapered wigglers with $\sin\psi_r = 0.2, 0.5$. The peak sideband growth for our chosen parameters was about $.5-.7\eta$ as compared to signal growth of $\eta\sin\psi_r$.

VI. Summary

We have studied the stability of sideband oscillations for a one-dimensional free electron laser. We perturb around a steady state ponderomotive equilibrium, characterized by an arbitrary distribution function $f_0(J)$ of trapped electrons travelling at mean velocity V. Here J, ϕ are the action-angle variables describing the motion of a trapped electron. $J=0$ corresponds to the bottom of the well and usually $\partial f_0/\partial J < 0$. The assumption $\partial f_0/\partial\phi = 0$ would be valid for a wiggler of many synchrotron periods. In such an equilibrium, we parametrize the strength of the taper by $S \equiv \sin\psi_r$ where $S=0$ corresponds to an untapered wiggler and $S=1$ is the maximum taper for which a well exists. In such a wiggler the laser signal grows

with a characteristic inverse growth length given by ηS with

$$\eta \equiv \frac{2\pi n_0 e^2 a_w}{m\gamma\omega a_0}$$

specifying the magnitude of the beam current. ω is the laser frequency, n_0 is electron density, and a_w and a_0 are the magnitudes of the wiggler and signal vector potentials, $a = eA/mc^2$.

Such an equilibrium may be susceptible to sideband instabilities which have a spatio-temporal variation proportional to $\exp[i\lambda(t - z/V) - \kappa Z]$. A κ with positive imaginary part for real λ corresponds to the growth along the wiggler of coupled sidebands with frequencies $\omega \pm \lambda$. The imaginary part of κ specifies the inverse growth length for the sidebands in excess of the signal growth length given above.

In general the unstable sidebands will have growth of order η and will lie in the frequency range

$$\frac{\Omega_0}{(1 - V_g/V)} \gtrsim \lambda \gtrsim -\frac{\Omega_0}{(1 - V_g/V)}.$$

Here V_g is the group velocity of the laser, and Ω_0 ($\Omega_0^2 \equiv \omega^2 a_w a_0 (1 + a_w^2)/\gamma_r^4$) the synchrotron frequency. Usually $1 = V_g > V$ but for guided microwaves it may be possible to reduce the group velocity so that $1 - V_g/V$ vanishes, removing the slippage which drives the sidebands.

In general we find that essentially all equilibria are unstable to sideband growth with inverse growth length of order η, although as discussed in detail below we have only been able to give a complete analysis for some cases. Growth rates for these cases are given in the text. We stress that what is relevant is the λ leading to fastest growth.

The general dispersion relation is given by Eq. (32). We discuss the following special cases.

A. Particles trapped at the bottom of the well

Here $f_0(J) = \delta(J)$ and Eq. (32) reduces to an algebraic dispersion relation Eq. (33). A Nyquist analysis then shows that such a tapered wiggler is always unstable unless $1 - V_g/V \equiv$

0 or more precisely $\omega\left(1-\frac{V_g}{V}\right)^2 < \Omega\left(\frac{1}{V}-1\right)$ and $S < 1/\sqrt{2}$. The detailed criterion is given in Eq. (45) with growth rates for various cases discussed thereafter.

B. Untapered wiggler (arbitrary $f_0(J)$) $S = 0$

Here the general necessary and sufficient stability criterion is given by Eq. (66). Except for cases with very small $1-V_g/V$ and rather special distributions, instability is always found. A particular case of interest, the uniformly filled bucket distribution ($f_0(J) \equiv 1$ for all trapped electrons) is discussed analytically with growth rates shown in Fig. 8. Results are close to those obtained previously.

C. Tapered wiggler, arbitrary $f_0(J)$, small λ, $S \neq 0$

In the limit of small λ^2 (implying small κ) we find Eq. (90) as a sufficient condition for instability. Of course, it is possible for small λ to be stable while higher frequencies

$$\lambda \sim O\left(\frac{\Omega_0}{1-V_g/V}\right)$$

remain unstable. Indeed our analysis discussed in A and B leads us to suspect this is so, even when the necessary condition for stability at small λ^2 is satisfied. Nonetheless analytic complexity limits our discussion to the small λ^2 limit.

Discussion of Eq. (90) is further split into two cases.

1. Normal slippage $(1-V_g/V)^2 > (1-V_g)\,\Omega_0^2/\eta\omega$

Here the governing stability relations are given in Eqs. (92) and (93). Analysis of these relations show that except for very nearly uniform distributions ($f_0(J) = 1$) and $S < .12$ the necessary condition for stability is violated. This very particular case is also presumably unstable as it lies close to the filled bucket $S = 0$ case discussed in B above but we have not rigorously proved this to be the case.

2. $(1 - V_g/V)^2 < (1 - V_g)\,\Omega_0^2/\eta\omega$

For this case we have not made great analytic progress. We find the stability conditions (95) and (96). These show possible stability for cases where electron distributions are concentrated near $J = 0$ and where $S < .5$. From the analysis given in A we suspect that a high-frequency instability is actually present but this is not proven and is perhaps worth more study.

Detailed numerical particle simulations have been made for cases B and C1. The growth rates found are shown in Fig. 9 and agree well with analytic predictions.

In summary we have shown that virtually all tapered and untapered FEL equilibria are subject to sideband instabilities whose growth rate is of the order of, but exceeds by a numerical factor of order $(1+.5/S)$, the signal growth rate. Note that for small S the growth rate of the sidebands as given by this approximate formula is $.5\eta$. For the special case C2 given above, this assertion is somewhat conjectural.

Acknowledgments

We would like to acknowledge many useful discussions with N. M. Kroll and M. L. Sloan during the course of this investigation. This research was supported by U. S. Dept. of Energy Contract No. DE-FG05-80ET-53088.

References

1. N. M. Kroll, P. L. Morton, and M. N. Rosenbluth, IEEE J. Quantum Elec. QE-17, 1436 (1981).

2. J. C. Goldstein and W. B. Colson, in *Proceedings of the International Conference on Lasers* (STS, McLean, Virginia, 1982), p. 218.

3. A. T. Lin in *Physics of Quantum Electronics*, edited by S. F. Jacobs, G. T. Moore, H. S. Pillof, M. Sargent III, M. O. Scully, and R. Spitzer (Addison-Wesley, Reading, Massachusetts, 1982), Vol. 9, p. 409.

4. W. B. Colson and R. A. Freedman, Optics Comm. **46**, 37 (1983).

5. J. C. Goldstein, in *Free-Electron Generators of Coherent Radiation*, edited by Charles A. Brau, Stephen F. Jacobs, and Marian O. Scully, (SPIE, Bellingham, WA, 1984) Vol. 453, p. 2.

6. C. M. Tang and P. Sprangle, in *Free-Electron Generators of Coherent Radiation*, edited by Charles A. Brau, Stephen F. Jacobs, and Marian O. Scully, (SPIE, Bellingham, WA, 1984) Vol. 453, p. 1.

7. M. N. Rosenbluth, H. Vernon Wong, and B. N. Moore, in *Free-Electron Generators of Coherent Radiation*, edited by Charles A. Brau, Stephen F. Jacobs, and Marian O. Scully, (SPIE, Bellingham, WA, 1984) Vol. 453, p. 25.

8. R. A. Freedman and W. B. Colson, Optics Comm. **52**, 409 (1985).

9. D. C. Quimby, J. M. Slater, and J. P. Wilcoxon, IEEE J. Quantum Electronics QE-21, 979 (1985).

10. W. M. Fawley and E. T. Scharlemann, private communication.

11. See also National Technical Information Service document AD-A158229/5 [ARA Report No. I-ARA-84-U-121 by M. N. Rosenbluth, H. Vernon Wong, B. N. Moore, and G. I. Bourianoff, December, 1984]. Copies may be ordered from the National Technical Information Service, Springfield, Virginia 22161. The price is MF $8.00 plus a $3.00 handling fee.

12. R. W. Warren, B. E. Newman, J. G. Winston, W. E. Stein, L. M. Young, and C. A. Brau, IEEE Journal of Quantum Electronics QE-19, 391 (1983).

13. F. G. Yee, J. Masud, T. C. Marshall, and S. P. Schlesinger, Nucl. Instrum. Methods A259, 104 (1987).

14. See also National Technical Information Service document AD-A136333/2 [ARA Report No. I-ARA-83-U-62 by M. N. Rosenbluth, H. V. Wong, and B. N. Moore, November, 1983]. Copies may be ordered from the National Technical Information Service, Springfield, Virginia 22161. The price is MF $8.00 plus a $3.00 handling fee.

15. R. C. Davidson, Phys. Fluids **29**, 2689 (1986).

16. W. M. Sharp and S. S. Yu, private communication.

17. R. C. Davidson and J. S. Wurtele, Phys. Fluids **30**, 557 (1987).

18. T. M. Antonson, Jr. and G. Laval, Phys. Fluids **B1**, 1721 (1989).

19. S. S. Yu, W. M. Sharp, W. M. Fawley, E. T. Scharlemann, A. M. Sessler, and E. J. Sternbach, Nucl. Instrum. Methods A259, 219 (1987).

20. J. Masud, T. C. Marshall, S. P. Schlesinger, F. G. Yee, W. M. Fawley, E. T. Scharlemann, S. S. Yu, A. A. Sessler, E. J. Sternbach, Phys. Rev. Lett. **58**, 763 (1987).

21. W. L. Kruer, J. M. Dawson, and R. N. Sudan, Phys. Rev. Lett. **23**, 838 (1969).

22. W. B. Colson, in *Physics of Quantum Electronics* (Addison-Wesley Publishing Company, Inc., Reading, MA, 1978), Vol. 5, p. 157.

23. M. Abramowitz and I. A. Stegun, Editors, *Handbook of Mathematical Functions* (Dover Publications, Inc., New York, NY, 1970), p. 567.

Table I. Variation of sideband gain $\mathrm{Im}(\delta/\eta)$ with wavenumber κ.

$\frac{\kappa}{\Omega_0}$	$\mathrm{Im}\left(\frac{\delta}{\eta}\right)$
0.2	0.059
0.4	0.196
0.6	0.332
0.8	0.412
1.0	0.428
1.2	0.393
1.6	0.265
2.0	0.147

Figure Captions

1. Ponderomotive potential well $V_p(\psi)$.

2. Plot of $Y_1(\kappa)$ (Eq. (35)) as a function of κ.

3. Plot of $Y_2(\kappa)$ (Eq. (36)) as a function of κ.

4. Contour of $G(\kappa)$ (Eq. (41)) as κ varies from $\kappa = -\infty$ to $\kappa = +\infty$ along the real axis. (Tapered wiggler-particles at the bottom of the well.)

5. Contour of $G(\kappa)$ (Eq. (63)) as κ varies from $\kappa = -\infty$ to $\kappa = +\infty$ along the real axis. The contour does not encircle the origin, implying one unstable root $D(\kappa) = 0$.

6. Contour of $G(\kappa)$ (Eq. (63)) as κ varies from $\kappa = -\infty$ to $\kappa = +\infty$ along the real axis. The contour encircles the origin in the negative sense, implying no unstable roots $D(\kappa) = 0$.

7. (a) Plot of $P_0\left(\hat{J}\right)$ (Eq. (72)) as a function of $\hat{J} = J/J_{\max}$.

   (b) Plot of P_0' (Eq. (73)) as a function of $\hat{J}$.

8. Plot of sideband gain $\mathrm{Im}(\delta/\eta)$ as a function of κ/Ω_0—uniformly filled bucket.

9. Plot of linear sideband gain $\mathrm{Im}(\delta/\eta)$ as a function of κ/Ω_0 for $f_0(J) = 9\pi\left(1 - k^2(J)\right)/32\Omega_0$ together with results of a 1-D particle simulation code.

10. Plot of $Q\left(\hat{J}, \sin\psi_r\right)$ (Eq. (93)) as a function of $\hat{J}$ for several values of $\sin\psi_r$.

11. Plot of $P\left(\hat{J}, \sin\psi_r\right)$ (Eq. (96)) as a function of $\hat{J}$ for several values of $\sin\psi_r$.

12. Electron and photon characteristic trajectories in the u–v plane.

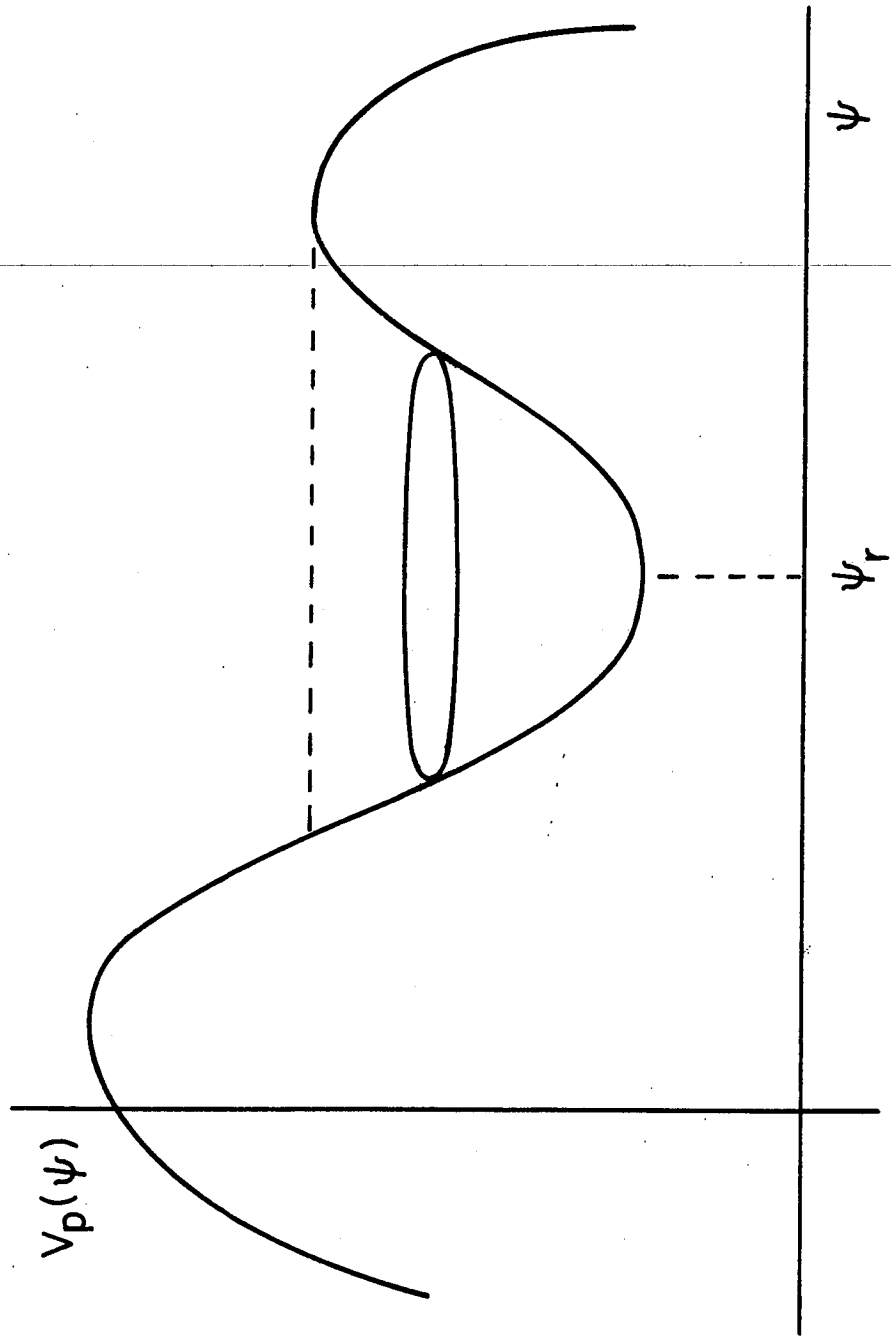

Figure 1

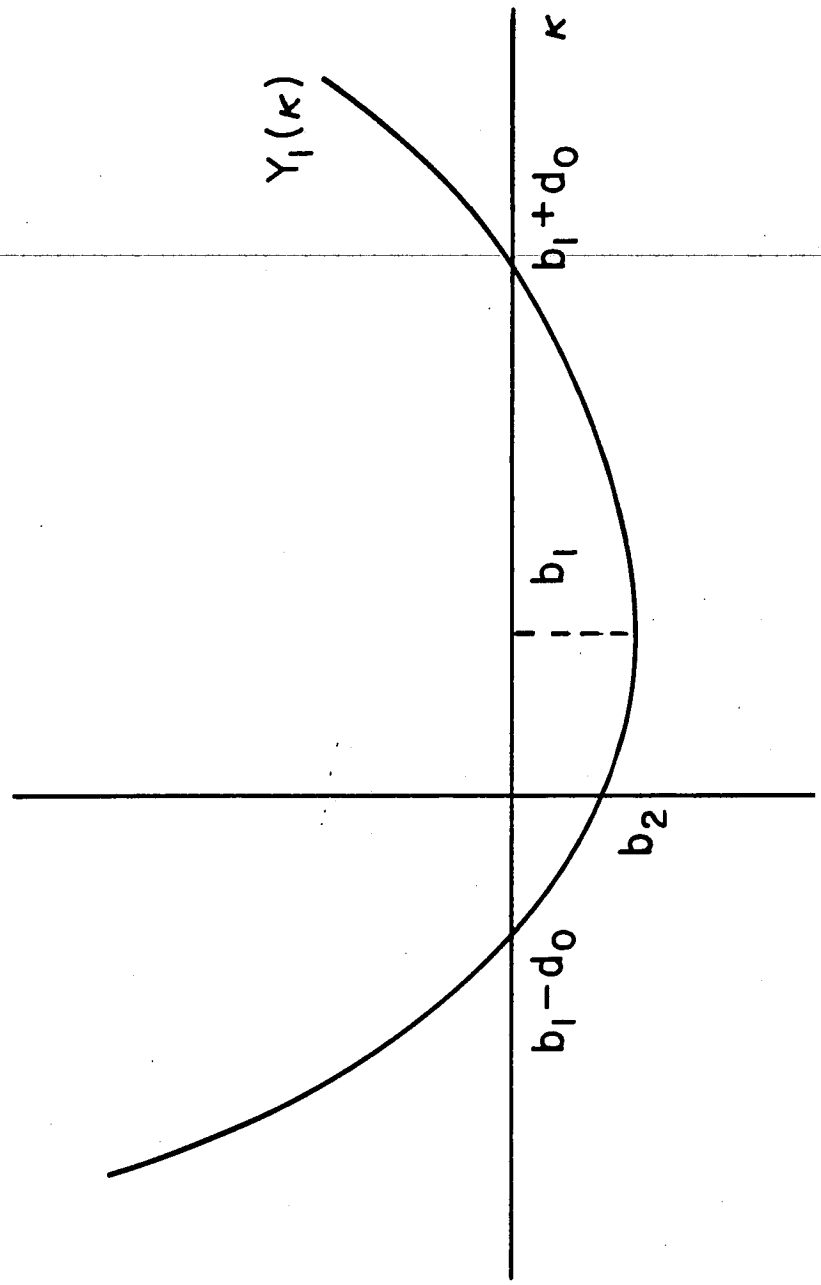

Figure 2

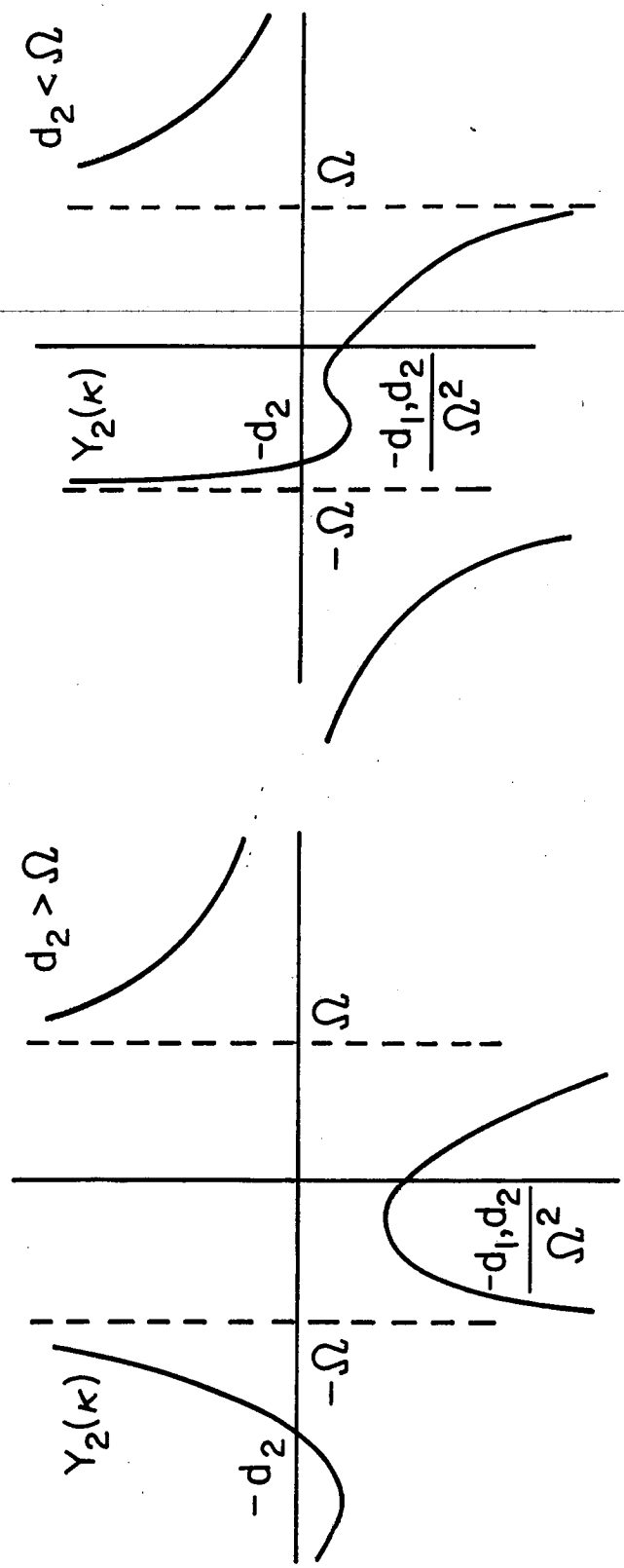
$d_2 < \Omega$
Ω
$Y_2(\kappa)$
$-d_2$
$\frac{-d_1 d_2}{\Omega^2}$
$-\Omega$
$d_2 > \Omega$
Ω
$\frac{-d_1 d_2}{\Omega^2}$
$-\Omega$
$Y_2(\kappa)$
$-d_2$

Figure 3

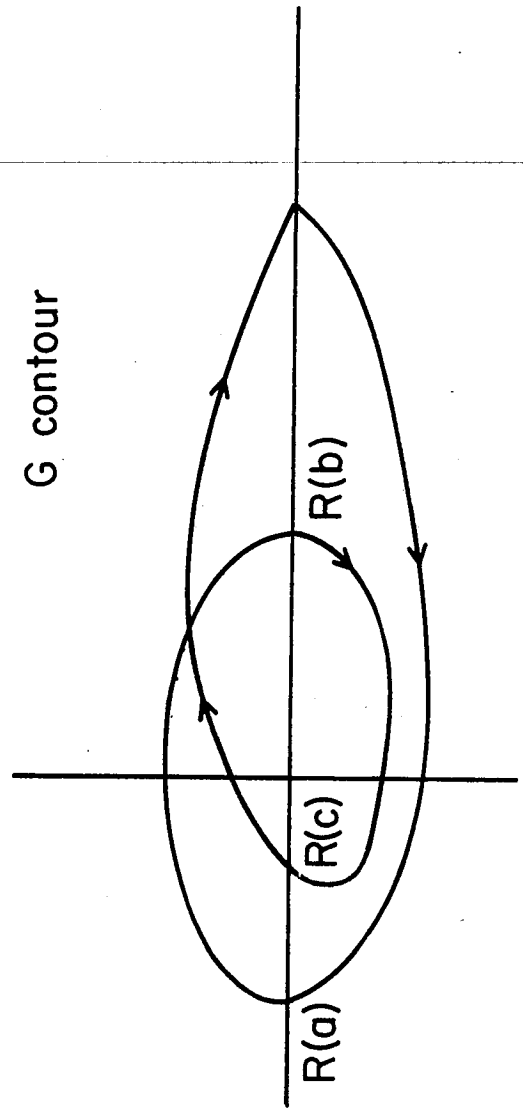

Figure 4

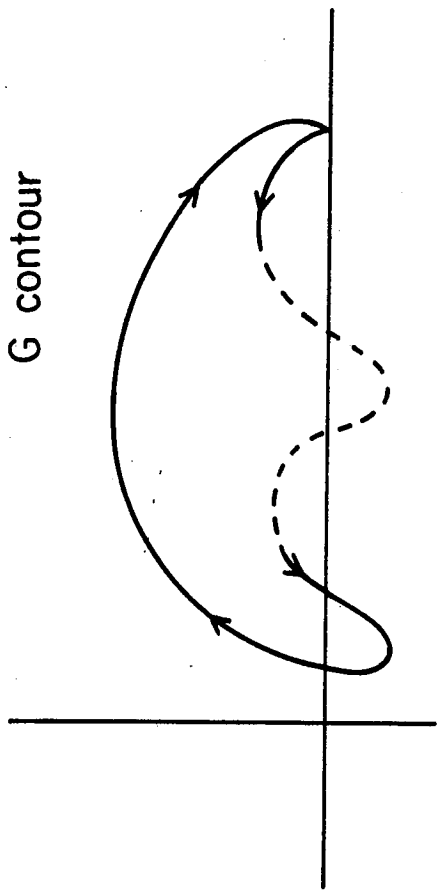

Figure 5

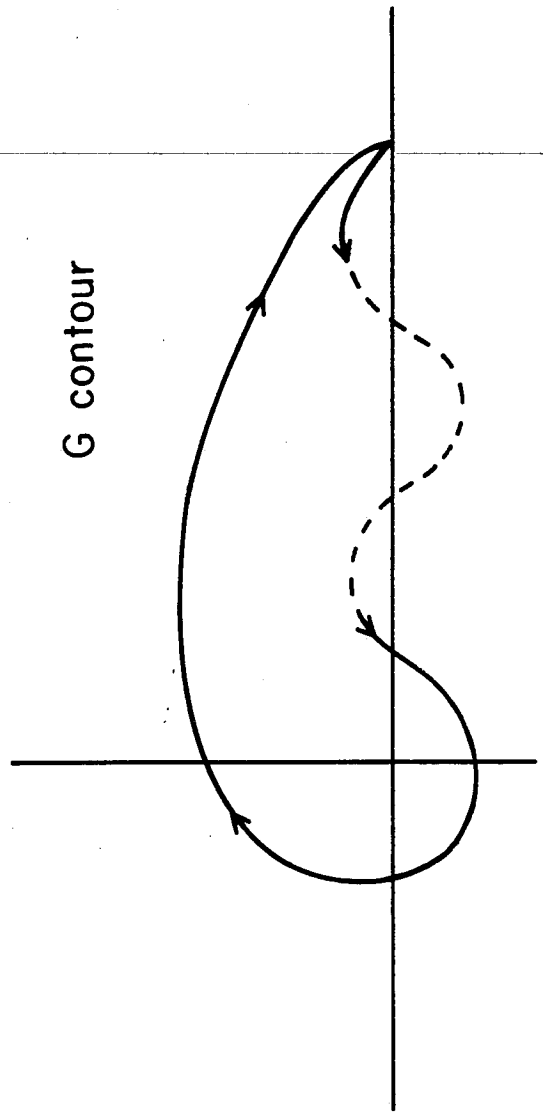

Figure 6

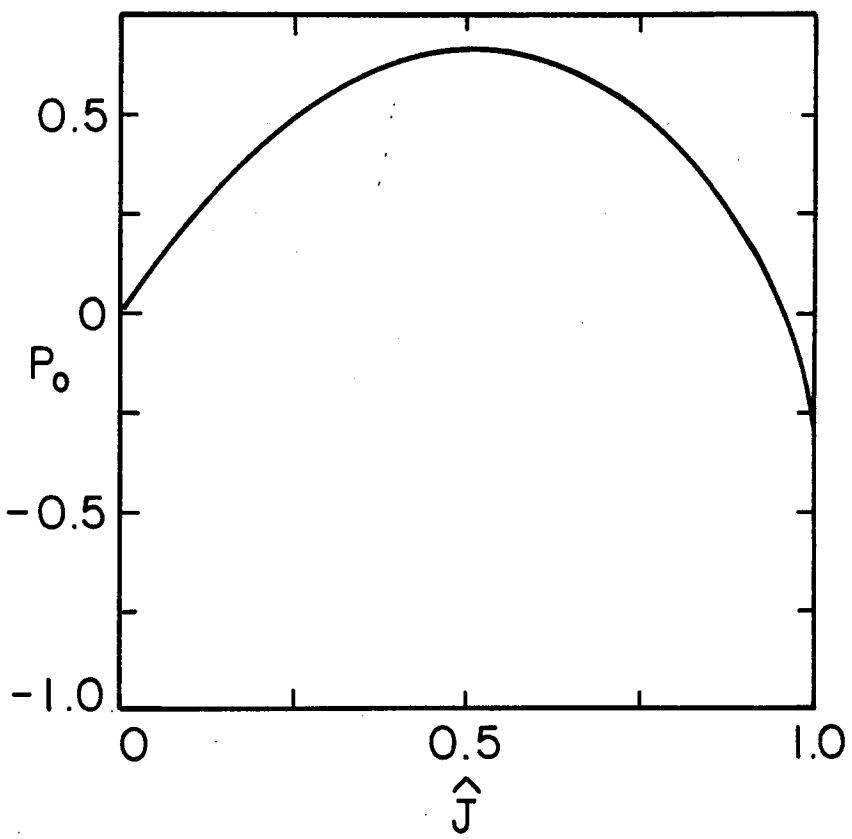

Figure 7a

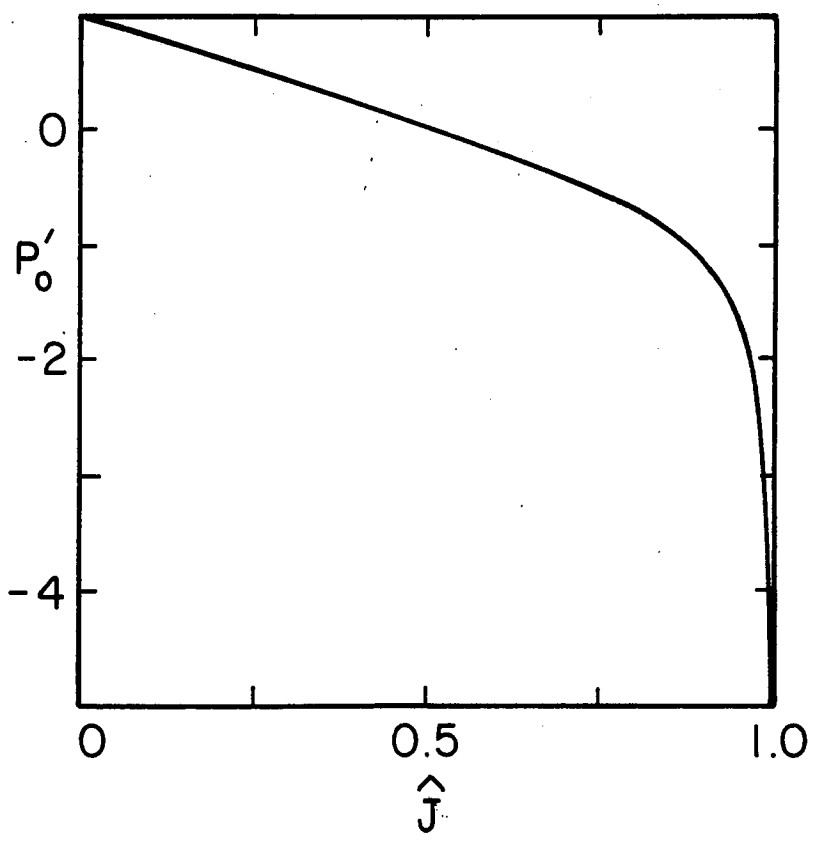

Figure 7b

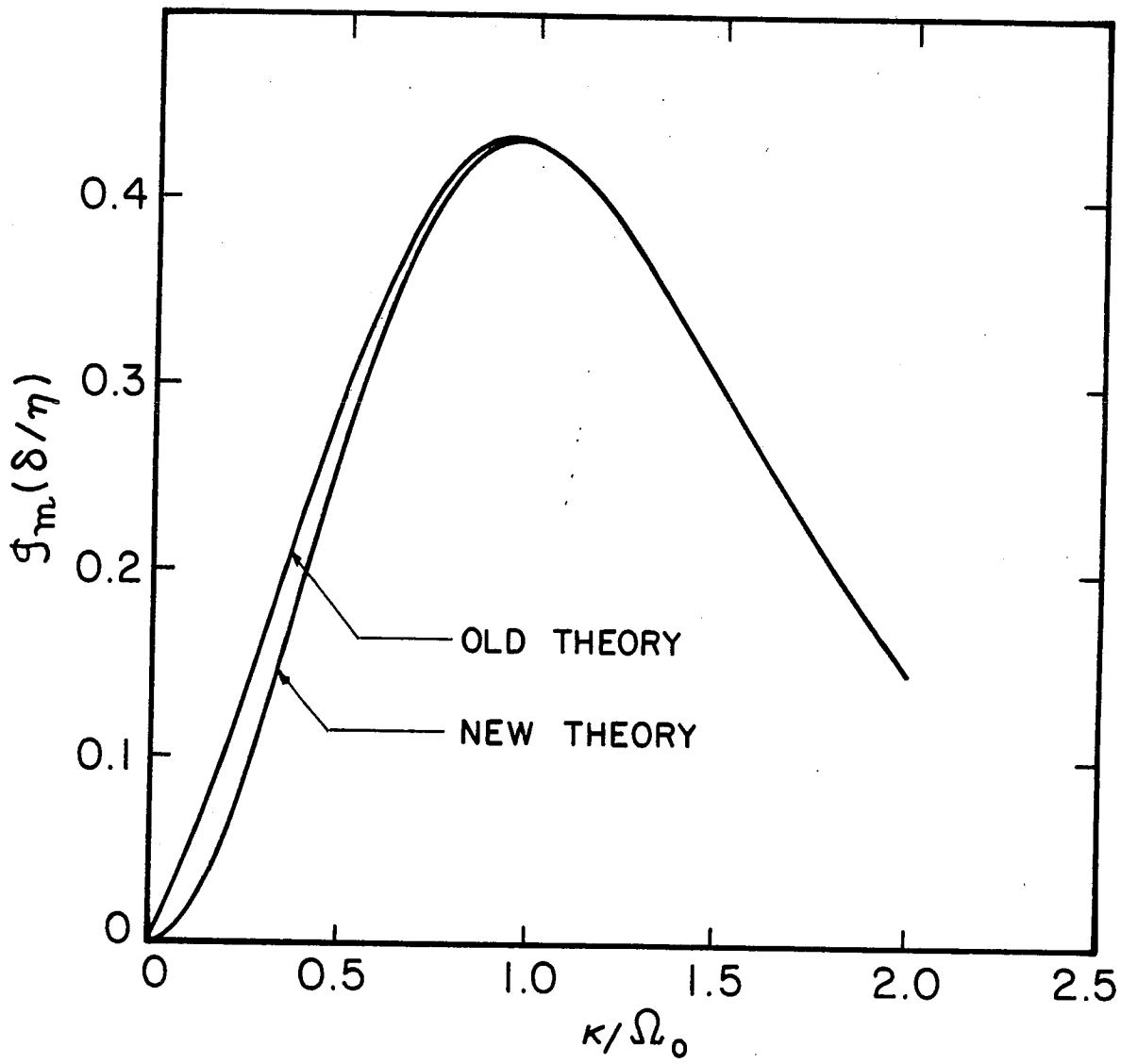
0.4
0.3
0.2
0.1
0
$\mathcal{F}_m(\delta/\eta)$
OLD THEORY
NEW THEORY
0
0.5
1.0
1.5
2.0
2.5
κ/Ω_0

Figure 8

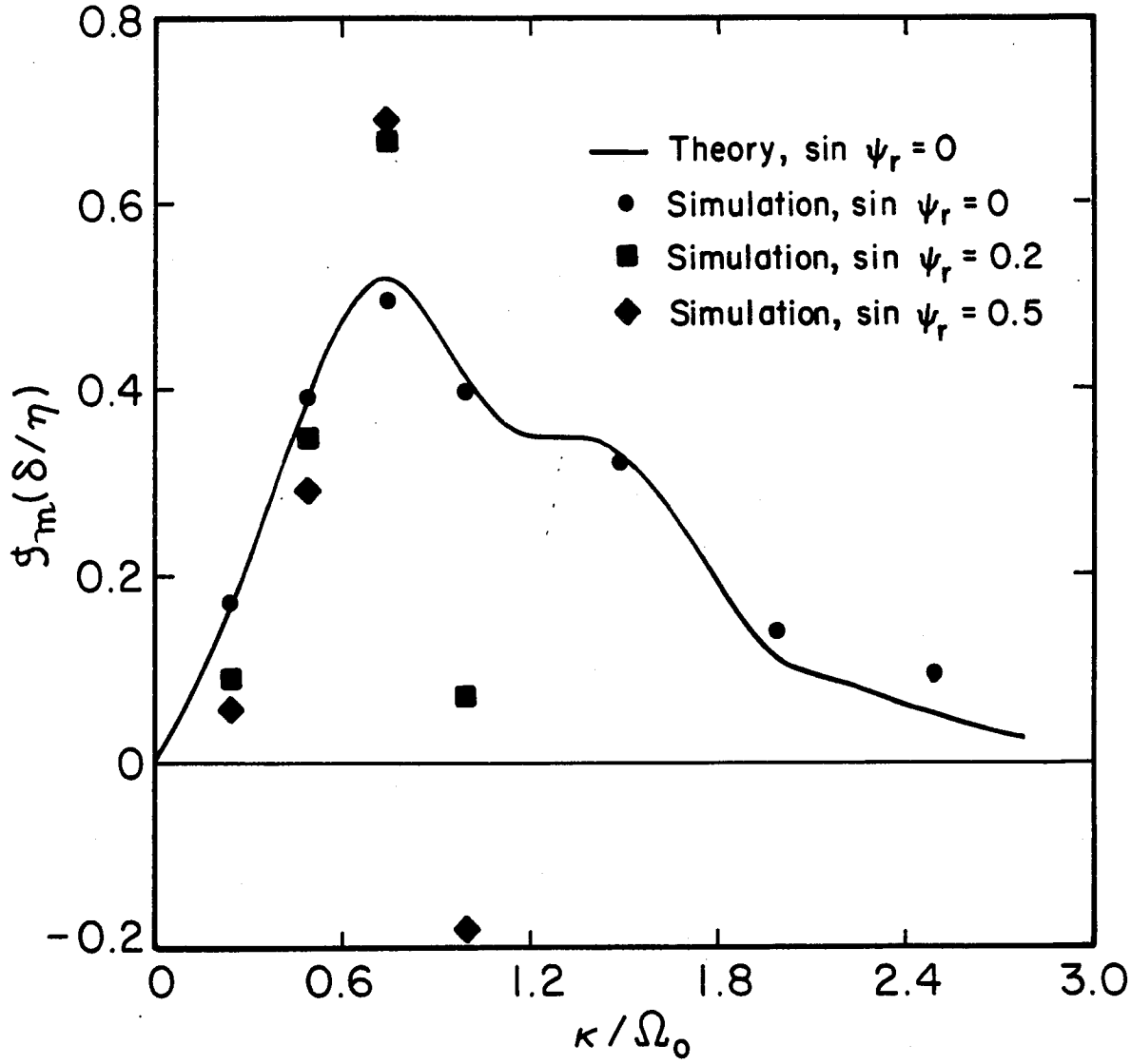
0.8
0.6
0.4
0.2
0
-0.2
0
0.6
1.2
1.8
2.4
3.0
κ / Ω_0
$\mathcal{F}_m(\delta/\eta)$
Theory, sin $\psi_r = 0$
Simulation, sin $\psi_r = 0$
Simulation, sin $\psi_r = 0.2$
Simulation, sin $\psi_r = 0.5$

Figure 9

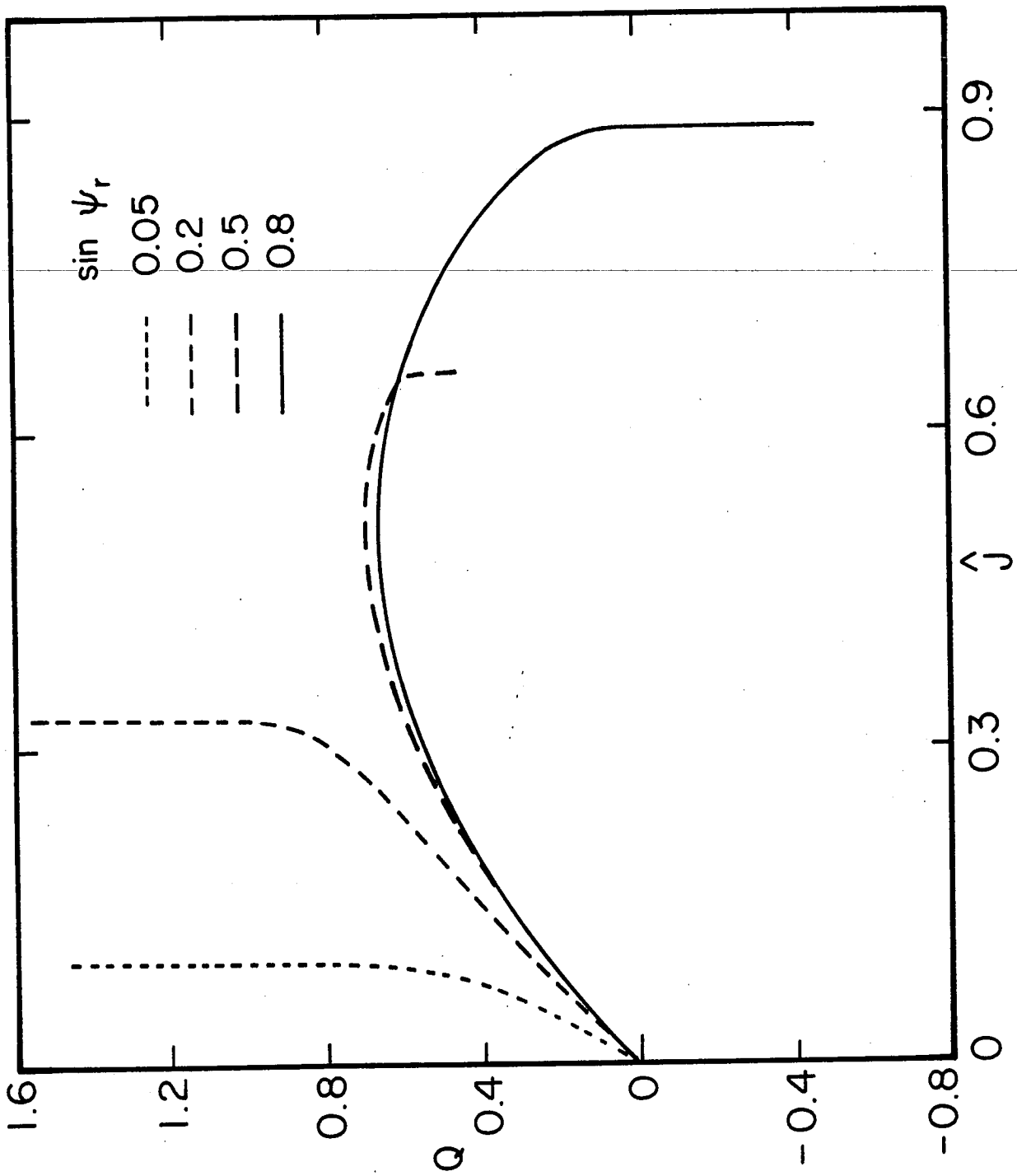

Figure 10

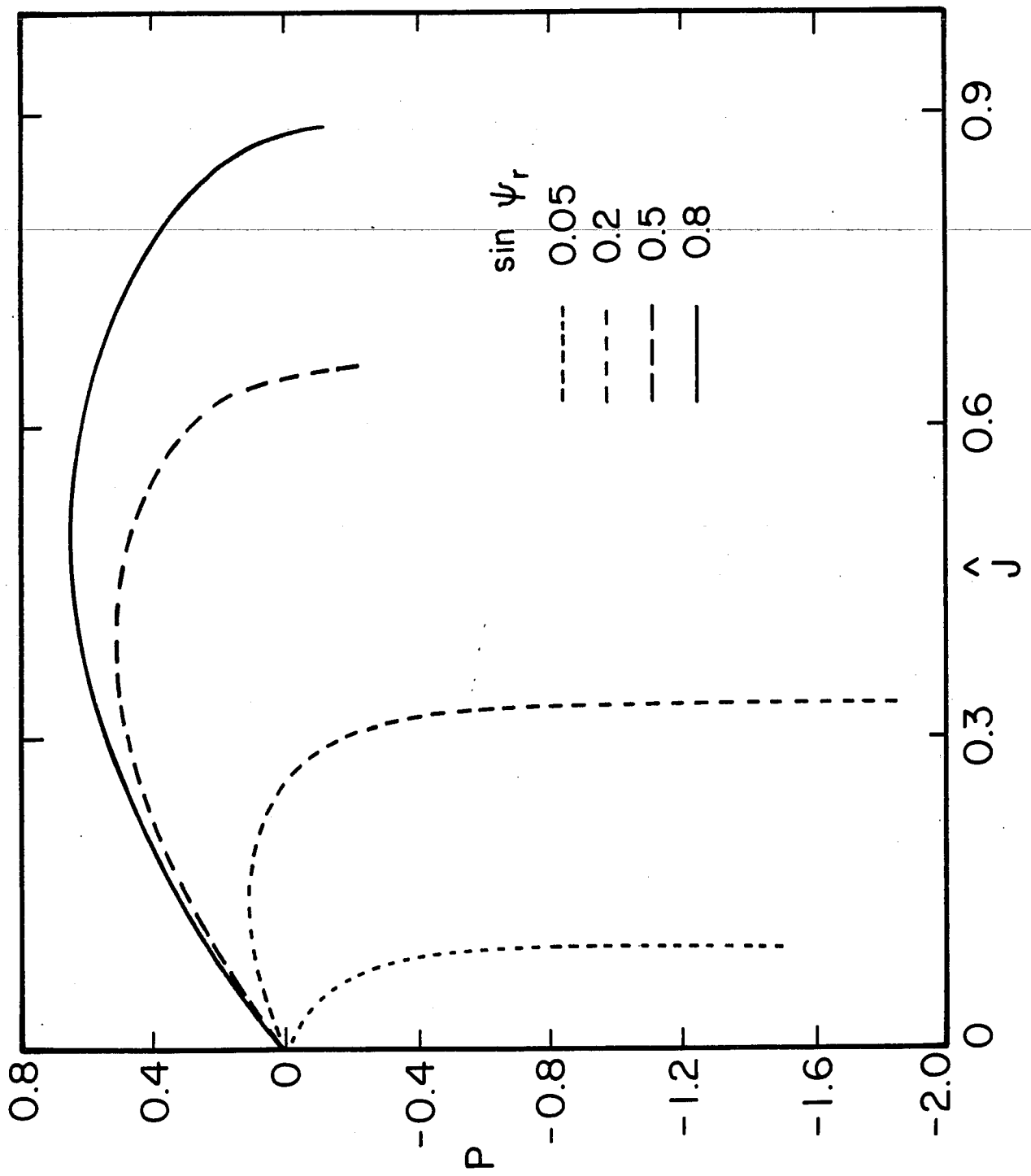

Figure 11

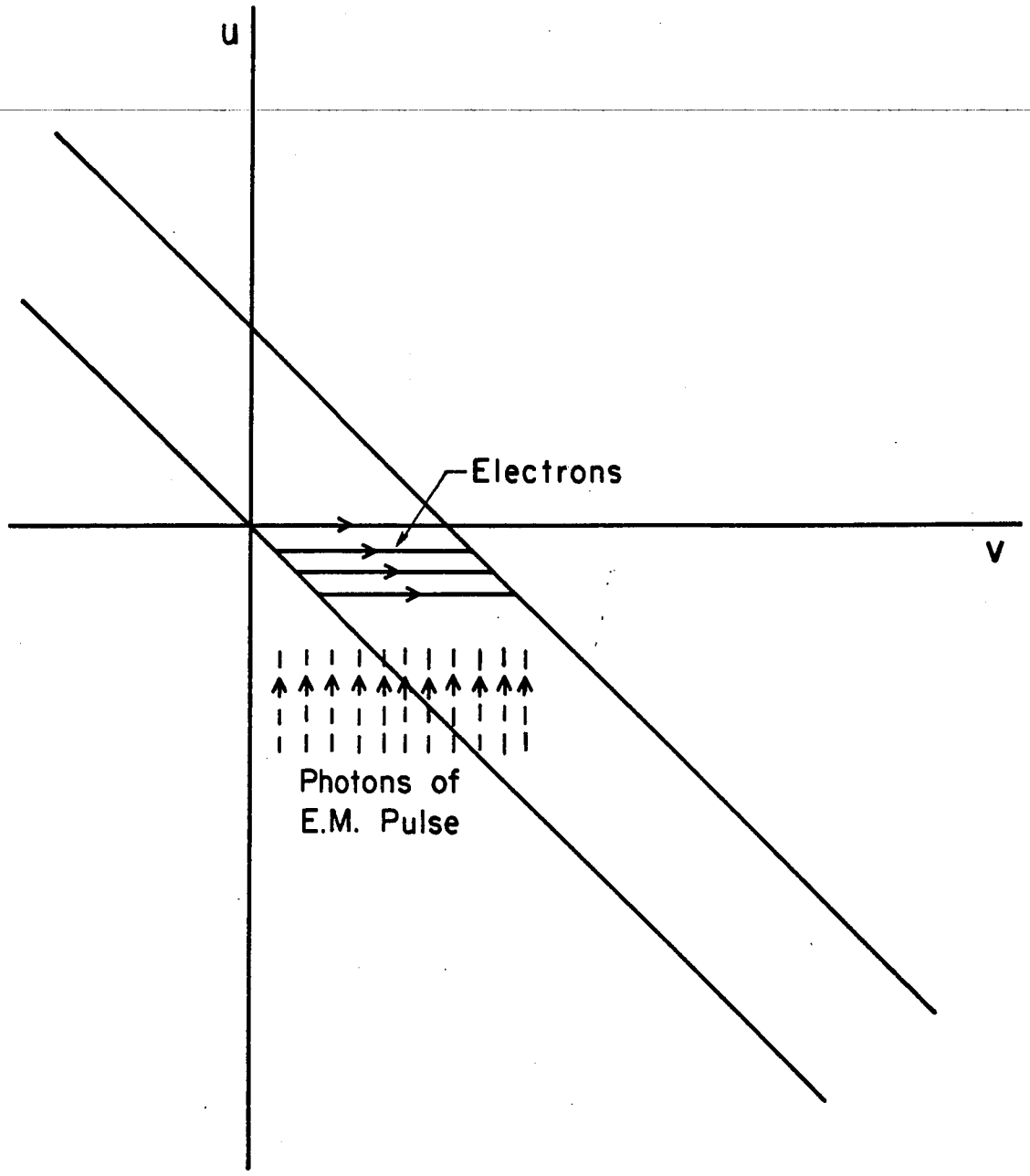

Figure 12